Chapter 4
Recent Advances in Electrowetting Microdroplet Technologies

Robert W. Barber and David R. Emerson

4.1 Introduction

The ability to handle small volumes of liquid, typically from a few picolitres (pL) to a few microlitres (μL), has the potential to improve the performance of complex chemical and biological assays [1–6]. The benefits of miniaturisation are well documented [7–9] and include smaller sample requirements, reduced reagent consumption, decreased analysis time, lower power consumption, lower costs per assay and higher levels of throughput and automation. In addition, miniaturisation may offer enhanced functionality that cannot be achieved in conventional macroscale devices, such as the ability to combine sample collection, analyte extraction, preconcentration, filtration and sample analysis onto a single microfluidic chip [10]. Microfluidics-based lab-on-a-chip devices have received considerable attention in recent years, and are expected to revolutionise clinical diagnostics, DNA and protein analysis and many other laboratory procedures involving molecular biology [11–13]. Currently, most lab-on-a-chip devices employ continuous fluid flow through closed microchannels. However, an alternative approach, which is rapidly gaining popularity, is to manipulate the liquid in the form of discrete, unit-sized microdroplets—an approach which is often referred to as *digital microfluidics* [14–18]. The use of droplet-based microfluidics offers many benefits over continuous flow systems; one of the main advantages is that the reaction or assay can be performed sequentially in a similar manner to traditional (macroscale) laboratory techniques. Consequently, a wide range of established chemical and biological protocols can be transferred to the micro-scale without the need to establish continuous flow protocols for the same reaction. In addition, droplet-based systems avoid many of the problems associated with single-phase microfluidics such as sample cross-contamination and diffusional dilution.

R.W. Barber (✉) • D.R. Emerson
Centre for Microfluidics and Microsystems Modelling, STFC Daresbury Laboratory, Warrington WA4 4AD, UK
e-mail: robert.barber@stfc.ac.uk

P. Day et al. (eds.), *Microdroplet Technology: Principles and Emerging Applications in Biology and Chemistry*, Integrated Analytical Systems,
DOI 10.1007/978-1-4614-3265-4_4,

One of the most important consequences of miniaturisation is the increase in the surface-to-volume ratio of the fluid. For example, the surface-to-volume ratio for a device with a characteristic length of 1 m is of order 1 m^{-1} whilst the surface-to-volume ratio for a microfluidic device having a characteristic length of 1 μm will increase to 10^6 m^{-1}. In other words, the surface-to-volume ratio of the fluid scales according to the inverse of the characteristic length [8]. Consequently, as devices are reduced in size, inertial forces will decrease while viscous effects and surface energies will become increasingly important. In the case of submillimetre-sized liquid droplets, capillary forces dominate the motion [19]. Under these circumstances, the control of the surface energy provides a useful tool for manipulating droplets [20–23]. Although chemical and topographical patterning of substrates has received considerable attention in recent years [24–26], the static nature of these surface treatments prevents the *active* control of droplets, as required in a fully-controllable digital microfluidic system. As a consequence, considerable work has been dedicated to the development of techniques that allow the wettability of the substrate to be varied both spatially and temporally. The most promising droplet actuation technique for digital microfluidic applications appears to be electrowetting [27–32], although other mechanisms have been demonstrated including dielectrophoresis [33–35], thermocapillary actuation [36–38] and optoelectrowetting [39–43]. In addition, other promising droplet handling techniques such as surface acoustic wave (SAW) actuation have been developed [44–47] although in this case, the droplet movement is achieved via the creation of acoustic waves rather than by changing the wettability of the surface. Furthermore, electrowetting can be combined with electrophoresis/dielectrophoresis, to provide a method for particle separation or sample enrichment [48–51], or can be used to collect or separate magnetic particles [52–54].

Over the last few years, electrowetting has become an increasingly important technology for droplet manipulation. Electrowetting can commonly achieve contact angle variations of more than 40° and the switching cycles can be performed hundreds of thousands of times without any detrimental effects to either the fluid or the chip. The switching response time for millimetre-sized droplets is relatively fast (typically several milliseconds) and is only limited by the inertia of the droplet rather than the switching time of the equilibrium contact angle [31]. Within just a few years, a rapidly expanding community of researchers has taken the concept of electrowetting from the initial research stage into fully-integrated digital microfluidic devices that are capable of complex chemical and biological assays [55–57].

4.2 Theory of Electrowetting

The phenomenon of electrocapillarity (or electrowetting) was first described by Lippmann [58] in 1875 when he showed that the capillary depression of mercury in contact with an electrolyte solution could be controlled by the application of a voltage.

As well as formulating the basic theory for electrocapillarity, he also proposed several practical devices that made use of the phenomenon, including a very sensitive electrometer which was later used to record the world's first electrocardiogram (ECG). Unfortunately, the application of electrowetting to aqueous electrolytes is severely restricted due to the electrolytic decomposition of water beyond a few hundred millivolts. In the 1990s, however, Berge [59] and Vallet et al. [60] realised that the problem of electrolysis could be overcome by the introduction of a thin insulating layer to separate the conductive liquid from the metal electrode. This concept is nowadays referred to as electrowetting-on-dielectric (EWOD) [61] or electrowetting-on-insulator-coated-electrodes (EICE) [28] and involves applying a voltage to modify the wetting behaviour of a conductive liquid in contact with a hydrophobic, insulated electrode. Thorough descriptions of electrowetting have been published by Mugele and Baret [31], Berthier [62] and Berthier and Silberzan [63] whilst investigations into the types of liquids that can be transported by EWOD have been conducted by Pollack [64], Srinivasan [65] and Chatterjee et al. [66].

In most practical electrowetting applications, the droplets reside on a horizontal planar substrate and are usually composed of aqueous solutions with a typical droplet diameter of 1 mm or less. The medium surrounding the droplet can either be air or another immiscible liquid such as silicone oil. However, recent work by Brassard et al. [67] has shown that it is possible to use an alternative mode of operation where the aqueous droplet is enclosed in a thin layer of oil which in turn is surrounded by air; this technique is referred to as *water-oil core-shell* droplets.

The relative importance of the gravitational force to the surface tension force can be expressed by the Bond number [62], $Bo = \Delta\rho g R^2/\sigma_{\mathrm{lv}}$ where $\Delta\rho$ is the difference in density between the droplet and the surrounding medium, g is the acceleration due to gravity, R is the radius of curvature of the droplet, and σ_{lv} is the *liquid-vapour* surface tension. (The Bond number is sometimes referred to as the Eötvös number, *Eo*.) In most electrowetting applications, the Bond number is usually less than unity [62], implying that gravitational forces are small in comparison to the surface tension force; it is therefore appropriate to ignore gravity in electrowetting applications [31].

In the absence of an external electric field, the shape of the droplet is determined solely by the surface tension, according to standard equilibrium theory (Young's equation) [62]. As shown in Fig. 4.1a, a surface tension (a force per unit length or an energy per unit area) is associated with the interface between each of the three phases; the *solid* substrate (s), the *liquid* droplet (l) and the surrounding ambient phase, which for simplicity is often denoted as *vapour* (v). Each interface exerts a force on the three-phase contact line, and the balance between the interfacial surface tensions i.e. σ_{sv} (solid-vapour), σ_{sl} (solid–liquid) and σ_{lv} (liquid-vapour) must be in equilibrium:

$$\sigma_{\mathrm{sv}} - \sigma_{\mathrm{sl}} - \sigma_{\mathrm{lv}} \cos\theta_{\mathrm{eq}} = 0 \tag{4.1}$$

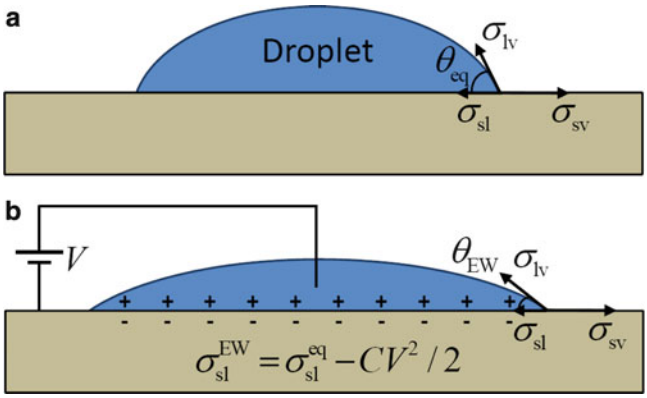

Fig. 4.1 A schematic diagram of wetting and electrowetting. (**a**) In the absence of an external electric field, the sum of the forces along the three-phase contact line must balance, leading to an equilibrium contact angle, θ_{eq}. (**b**) Application of a potential difference between the liquid and the substrate creates a capacitance, C, at the solid–liquid interface which causes the solid–liquid interfacial surface tension to be reduced by $CV^2/2$. This causes the droplet to spread and reduces the contact angle to θ_{EW}

where θ_{eq} is the *equilibrium* (or Young's) contact angle. Rearranging (4.1) yields the familiar form of Young's equation:

$$\cos\theta_{eq} = \frac{\sigma_{sv} - \sigma_{sl}}{\sigma_{lv}} \tag{4.2}$$

It should be noted that the vertical component of the surface tension force is balanced by normal stresses within the solid substrate [31].

Applying a potential difference, V, between the liquid and the substrate will change the shape of the droplet, as shown schematically in Fig. 4.1b. This is due to the fact that the solid–liquid interface effectively behaves as a parallel-plate capacitor, with a capacitance per unit area, C. The energy stored in the capacitor is $CV^2/2$ whilst the work done by the external supply voltage is $-CV^2$ and therefore the free energy of the droplet per unit interfacial area is reduced by $CV^2/2$. Application of the voltage therefore causes the solid–liquid interfacial surface tension to be reduced to $\sigma_{sl} - CV^2/2$ leading to a new force balance equation:

$$\sigma_{sv} - (\sigma_{sl} - CV^2/2) - \sigma_{lv}\cos\theta_{EW} = 0 \tag{4.3}$$

where θ_{EW} is the steady-state contact angle after the application of the *electrowetting* voltage. Combining (4.1) and (4.3) leads to the Lippmann-Young equation governing the contact angle of the droplet:

$$\cos\theta_{EW} = \cos\theta_{eq} + \frac{CV^2}{2\sigma_{lv}} \tag{4.4}$$

Equation (4.4) shows that the contact angle will decrease (i.e. the surface will become more hydrophilic) as the applied voltage increases.

Early electrowetting experiments were conducted with exposed metallic electrodes in direct contact with the conductive liquid or electrolyte. In this case, the potential difference between the liquid and electrode forms an electrical double layer at the solid–liquid interface. The specific capacitance (i.e. the capacitance per unit area) of the ionic double layer can be estimated by making the assumption that the counter-ions in the liquid are located at a fixed distance from the surface; this is sometimes referred to as the Helmholtz model [31, 62]. The specific capacitance of the electrical double layer is therefore given by

$$C_{\mathrm{H}} = \frac{\varepsilon_0 \varepsilon_{\mathrm{l}}}{\lambda_{\mathrm{D}}} \tag{4.5}$$

where ε_0 is the permittivity of free space ($\varepsilon_0 = 8.8541878 \times 10^{-12}$ F/m), ε_{l} is the relative permittivity of the conductive liquid and λ_{D} is the Debye screening length [68], typically in the nanometre range. Substituting (4.5) into the Lippmann-Young equation leads to

$$\cos\theta_{\mathrm{EW}} = \cos\theta_{\mathrm{eq}} + \frac{\varepsilon_0 \varepsilon_{\mathrm{l}} V^2}{2\lambda_{\mathrm{D}} \sigma_{\mathrm{lv}}} \tag{4.6}$$

As discussed by Mugele and Baret [31] and Berthier [62], it is sometimes necessary to modify the Lippmann-Young equation to account for the spontaneous charge which occurs when a conducting surface is immersed in an electrolyte:

$$\cos\theta_{\mathrm{EW}} = \cos\theta_{\mathrm{eq}} + \frac{\varepsilon_0 \varepsilon_{\mathrm{l}}}{2\lambda_{\mathrm{D}} \sigma_{\mathrm{lv}}} (V - V_{\mathrm{pzc}})^2 \tag{4.7}$$

where V_{pzc} is the potential difference at zero charge. Usually, the electrical double layer has a relatively high capacitance, and therefore large changes in contact angle can be achieved using relatively small applied voltages. Unfortunately, direct application of electrowetting using metallic electrodes is somewhat limited due to the electrolytic decomposition of the aqueous liquid above a certain voltage.

To overcome the problem of electrolysis, a thin dielectric layer can be used to insulate the conductive liquid from the electrode. The main advantage of EWOD over conventional electrowetting is that higher potential differences and, therefore, greater contact angle changes can be employed without any detrimental electrochemical reactions on the electrode. In addition, the surface of the microfluidic chip can be coated with highly hydrophobic compounds to enhance the contact angle changes due to electrowetting. A practical demonstration of EWOD-based actuation is shown in Fig. 4.2 [69] which illustrates the variation in the wettability of a water droplet on a Teflon surface.

With the introduction of a dielectric layer, the EWOD system is effectively composed of two capacitors in *series* with each other; namely, the capacitance due

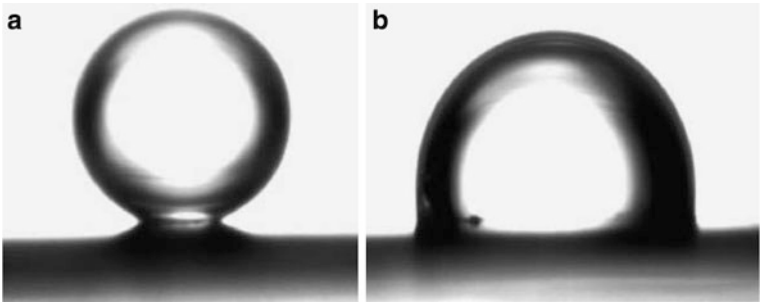

Fig. 4.2 Experimental visualisation of electrowetting clearly demonstrating the control of the contact angle: (**a**) in the absence of an external electric field, the water droplet exhibits a strong hydrophobic contact with the Teflon substrate (DuPont® AF 1600), (**b**) application of an electric potential of 80 V to the droplet causes a significant reduction in the contact angle. Reproduced from Berthier et al. [69] with kind permission from Elsevier

to the electrical double layer at the solid–liquid interface, C_H and the capacitance due to the dielectric layer, C_d which is given by

$$C_d = \frac{\varepsilon_0 \varepsilon_d}{d} \tag{4.8}$$

where ε_d is the relative permittivity of the dielectric layer and d is the thickness of the layer. Comparing (4.5) and (4.8) leads to

$$\frac{C_H}{C_d} = \frac{\varepsilon_l}{\varepsilon_d} \frac{d}{\lambda_D} \tag{4.9}$$

Since $d \gg \lambda_D$ and $\varepsilon_l > \varepsilon_d$ then $C_H \gg C_d$ i.e. the capacitance of the electrical double layer, C_H is usually much larger than the capacitance of the dielectric film, C_d. Since the capacitors are in series, the total specific capacitance, C, is given by

$$\frac{1}{C} = \frac{1}{C_H} + \frac{1}{C_d} \tag{4.10}$$

which can be approximated by $C \approx C_d$. Thus, for EWOD actuation, (4.6) is replaced by

$$\cos\theta_{EW} = \cos\theta_{eq} + \frac{\varepsilon_0 \varepsilon_d V^2}{2d\sigma_{lv}} \tag{4.11}$$

The last term on the right-hand side of (4.11) is sometimes referred to as the dimensionless electrowetting number, $\eta = \varepsilon_0 \varepsilon_d V^2/(2d\sigma_{lv}) = CV^2/(2\sigma_{lv})$ and is a measure of the relative importance of the electrostatic energy compared to the surface tension [31]. One of the disadvantages of EWOD is that the lower specific

capacitance of the dielectric layer requires significantly larger potentials to achieve a given reduction in contact angle. For example, considering a 1 μm thick dielectric layer composed of Teflon AF 1600 ($\varepsilon_d = 1.93$) with water as the conductive liquid ($\sigma_{lv} = 0.072\ \mathrm{N/m}$), gives a dimensionless electrowetting number of approximately $10^{-4}V^2$. This implies that external voltages of between 30 and 80 V [62] are required to create substantial reductions in the contact angle. One of the other disadvantages of using a dielectric layer is the fact that biomolecules can sometimes bind nonspecifically to the hydrophobic surface. Yoon and Garrell [70] have shown that biomolecular adsorption can be controlled by minimising the time during which the electrodes are switched off and also by carefully choosing the pH of the solution and the polarity of the electrodes. In addition, Luk et al. [71] have shown that low concentrations of Pluronic F127 can limit the extent of protein adsorption.

In practical EWOD applications, the substrate usually comprises of a metallic electrode, a dielectric layer (Parylene, SiO_2 or Si_3N_4) and a hydrophobic layer (spin-coated Teflon or plasma deposited SiOC). In some cases, the situation is further complicated by the fact that the dielectric layer is formed from a sandwich structure composed of $SiO_2/Si_3N_4/SiO_2$. The effective capacitance of the combined substrate (formed from n parallel layers) can be determined from the usual law for capacitors in series:

$$\frac{1}{C} = \sum_{i=1}^{n} \frac{1}{C_i} \tag{4.12}$$

The capacitance of the electrical double layer at the solid–liquid interface is usually neglected. However, direct calculation of the capacitance of the dielectric layer can sometimes be avoided by fitting the Lippmann-Young equation to experimental data of contact angle vs. applied voltage. This is usually done by plotting $(\cos\theta_{EW} - \cos\theta_{eq})$ against V^2. The gradient of the fitted line is equal to $C/(2\sigma_{lv})$ and therefore knowledge of the liquid-vapour surface tension, σ_{lv} leads to an estimate of the capacitance, C. This technique is sometimes preferred to direct computation, due to uncertainties in estimating the thickness and relative permittivities of the deposited layers.

A significant advantage of controlling the variation in the wetting angle via electrowetting, rather than by thermocapillary effects, is the speed with which the contact angle can be modified. Mugele and Baret [31] indicate switching times of typically several milliseconds, and this makes the technique potentially fast enough to be used in video display screens [72]. The manipulation and transport of droplets above a solid surface are equally as fast; velocities of between 1 and 100 mm/s have been reported [27, 29, 73, 74] while droplets have been shown to be split in less than 1 s [74]. Other potential applications for electrowetting include variable focal length liquid micro-lenses [75–77], dynamically tuneable fibre-optic devices which act as switches and waveguides [78, 79] and adaptive cooling of integrated circuits [80].

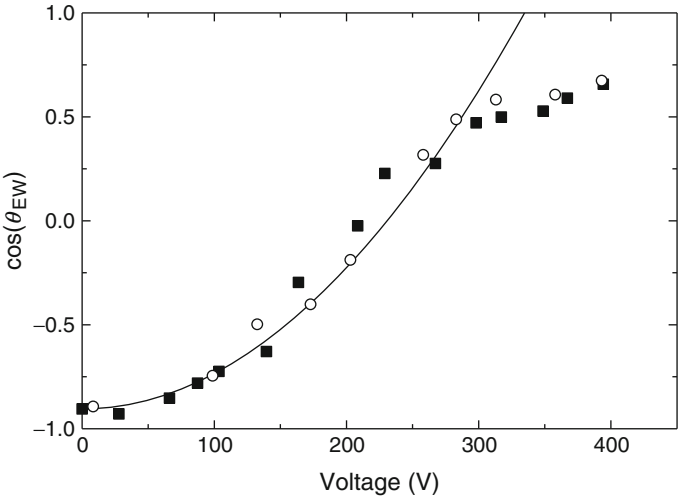

Fig. 4.3 Variation of measured contact angle vs. applied voltage for a glycerol-NaCl water droplet with silicone oil as the ambient medium and a 5 μm thick layer of Teflon AF 1601 as the dielectric. The *filled symbols* denote increasing voltage and the *open symbols* denote decreasing voltage. The *solid line* denotes the fitted parabolic variation in the value of $\cos\theta_{EW}$ as predicted by the Lippmann-Young law—(4.11). Adapted from Mugele and Baret [31] with permission from IOPscience 2005

4.2.1 Contact Angle Saturation and Dielectric Breakdown

An important observation that is common to all EWOD studies is that the contact angle variation in the Lippmann-Young equation is only valid below a critical threshold voltage, after which the electrowetting process *saturates* and the contact angle becomes independent of the applied voltage [81–84]. The essential features of contact angle saturation are illustrated in Fig. 4.3 which indicates that there is an effective upper limit to the electrowetting force, implying that it is impossible to achieve perfect wetting of $\theta_{EW} = 0$ ($\cos\theta_{EW} = 1$). However, Krupenkin et al. [85] have shown that it is possible to achieve complete wetting at voltages as low as 22 V, by using superhydrophobic nanostructured surfaces.

Although contact angle saturation is well documented [86, 87], the physical explanation for the saturation limit is not fully understood [62] and a number of different (and sometimes conflicting) theories have been developed to explain the phenomenon. Verheijen and Prins [88] have proposed that the injection of charges into the insulating layer at higher voltages causes a screening, or trapping effect, which reduces the density of the charges at the solid–liquid interface thereby weakening the electrowetting force. On the other hand, Vallet et al. [86] have explained the phenomenon by the ionisation of the air in the vicinity of the contact line. This reduces the electric charge density and prevents the electrowetting force increasing with applied voltage. However, Vallet et al.'s explanation assumes that

the droplet is surrounded by air and therefore cannot explain the occurrence of contact angle saturation when the droplet is surrounded by another liquid, such as silicone oil. Other researchers, such as Papathanasiou and Boudouvis [83], have explained the phenomenon by the presence of 'fringe' effects at the contact line. These fringe effects can increase the electric field strength in the dielectric by an order of magnitude, or more, causing breakdown in the dielectric, and leakage of electrical charge.

4.2.1.1 Modified Lippmann-Young Equation

Despite the lack of consensus as to the physical explanation for contact angle saturation, it is possible to derive a constitutive relationship for the contact angle variation in terms of the *saturation* contact angle, θ_s. At low voltages, the Lippmann-Young equation (4.4) indicates that there is a linear relationship between $\cos\theta_{EW}$ and V^2 whilst at large voltages, the contact angle asymptotes to a fixed value, θ_s. This situation is analogous to paramagnetism where the induced magnetic moment is a linear function of the magnetic field at small field strengths and asymptotes to the saturation limit at large field strengths. The work on paramagnetism was pioneered by Langevin in the early twentieth century and led directly to the so-called Langevin (or sometimes, Langevin-Debye) function, L, defined by

$$L(x) = \coth(3x) - \frac{1}{3x} \tag{4.13}$$

Berthier et al. [62, 63, 69] have shown that the Langevin function can be used to modify the standard Lippmann-Young equation to account for contact angle saturation. Firstly, the Lippmann-Young formula (4.4) is written in the following form:

$$\frac{\cos\theta_{EW} - \cos\theta_{eq}}{\cos\theta_s - \cos\theta_{eq}} = \frac{CV^2}{2\sigma_{lv}(\cos\theta_s - \cos\theta_{eq})} \tag{4.14}$$

The *modified* Lippmann-Young equation, accounting for contact angle saturation, can then be obtained by introducing the Langevin function into the right-hand side of (4.14) to give:

$$\frac{\cos\theta_{EW} - \cos\theta_{eq}}{\cos\theta_s - \cos\theta_{eq}} = L\left(\frac{CV^2}{2\sigma_{lv}(\cos\theta_s - \cos\theta_{eq})}\right) \tag{4.15}$$

Experimental evidence [69] suggests that the Langevin approximation provides a fairly accurate constitutive law for the variation of contact angle with applied electrical potential.

4.2.1.2 Dielectric Breakdown

If the electric field strength exceeds a critical value, denoted as E_{BD}, the dielectric will suddenly break down resulting in an electrically-conductive pathway through the material which degrades or even destroys the insulating properties of the dielectric layer. It is therefore necessary to ensure that the operating conditions within the EWOD system are below the critical value of the electric field strength. For a dielectric layer of thickness, d, the breakdown voltage, V_{BD} is related to the critical electric field strength, E_{BD} by

$$V_{BD} = E_{BD} d \tag{4.16}$$

Taking Teflon as an example insulator, the critical electric field strength is 60 V/μm. Thus, a 1.5 μm thick layer of Teflon should be able to withstand an applied voltage of just under 90 V. However, dielectric breakdowns are sometimes observed at voltages lower than theory would suggest; these are thought to be caused by defects in the dielectric layer or in the underlying substrate. In addition, anomalous dielectric breakdowns can occur when cells or proteins adhere to the dielectric layer [63]. In this case, geometrical inhomogeneities in the relative permittivity are thought to increase the local electric field strength causing dielectric breakdown.

The choice of dielectric thickness is crucial to the design of any EWOD system since the thickness not only affects the breakdown voltage but also the capacitance of the dielectric layer which in turn affects the dimensionless electrowetting number, η. Increasing the thickness of the dielectric layer reduces the electrowetting number which leads to larger electric potentials to achieve a given reduction in contact angle. A criterion for the dielectric thickness can be obtained by rearranging the Lippmann-Young relationship (4.11) in the following form:

$$V = \sqrt{\frac{2d\sigma_{lv}}{\varepsilon_0 \varepsilon_d}(\cos\theta_{EW} - \cos\theta_{eq})} \tag{4.17}$$

For a fixed reduction in the contact angle, it can be seen that the externally applied voltage, V, varies according to the square root of the dielectric thickness, d. However, to prevent dielectric breakdown, the thickness of the layer also needs to satisfy (4.16). Combining (4.16) and (4.17) then leads to a minimum dielectric thickness [62]:

$$d_{min} = \frac{2\sigma_{lv}}{\varepsilon_0 \varepsilon_d E_{BD}^2}(\cos\theta_{EW} - \cos\theta_{eq}) \tag{4.18}$$

If the dielectric layer is thinner than this limit, the voltage required to create the desired contact angle of θ_{EW} will cause the dielectric to break down.

4.2.2 Contact Angle Hysteresis

Experimental evidence indicates that electrowetting and thermocapillary processes exhibit dynamic hysteresis whenever the three-phase contact line is in motion [31, 62, 89, 90]. This is due to the different contact angles at the advancing and receding menisci. Increasing the applied voltage on a droplet reduces the solid–liquid interfacial surface tension, σ_{sl}, causing the droplet to spread; this situation gives rise to an *advancing* contact line. Conversely, when the voltage is decreased, the droplet will revert to its original (equilibrium) shape creating a *receding* contact line. Experimental observations indicate that, for a given electrowetting voltage, the advancing contact angle is always larger than the receding contact angle. The change in the contact angle away from the equilibrium (static) value can be defined as the *electrowetting hysteresis angle*, α. In the case of de-ionised water surrounded by silicone oil on an SiOC substrate, the hysteresis angle is typically between 1.5 and 2°. However, de-ionised water surrounded by air on a Teflon substrate has a much larger electrowetting hysteresis angle of between 7 and 9° [90]. Contact angle hysteresis can therefore have an important effect on EWOD-based droplet manipulation [91].

4.2.2.1 Minimum Actuation Potential

Contact angle hysteresis is responsible for the minimum or threshold potential that has frequently been observed when transporting droplets between different control electrodes [90]. It is informative to consider the motion of a droplet straddling two adjacent control electrodes, as shown schematically in Fig. 4.4. One of the control electrodes is assumed to be actuated whereas the other electrode is switched off. In the absence of contact angle hysteresis (i.e. $\alpha = 0$), the droplet would be able to move under the smallest of applied voltages. However, experimental evidence indicates that, in practice, the droplet will not begin to move until the electrical potential exceeds a certain threshold, $V_{\min}$. At the onset of droplet motion, the contact angle above the actuated electrode will be $\theta_{EW} + \alpha$ (i.e. an advancing contact line) whereas the contact angle above the non-actuated electrode will be $\theta_{eq} - \alpha$ (a receding contact line). The potential at the threshold of droplet motion can then be determined from the requirement that there must be a net positive electrowetting force towards the activated electrode, i.e.

$$\theta_{EW} + \alpha \leq \theta_{eq} - \alpha \Rightarrow \cos(\theta_{EW} + \alpha) \geq \cos(\theta_{eq} - \alpha) \tag{4.19}$$

This expression can be combined with the Lippmann-Young formula (4.4) to determine the minimum actuation potential, $V_{\min}$. It can readily be shown that

$$\frac{C}{2\sigma_{lv}} V_{\min}^2 = \tan\alpha[\sin\theta_{EW}(V_{\min}) + \sin\theta_{eq}] \tag{4.20}$$

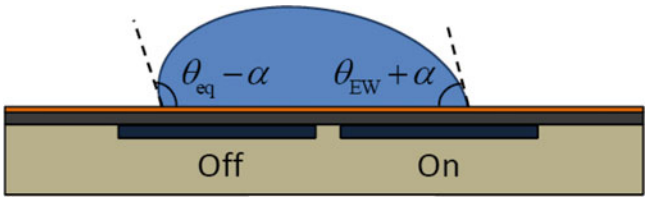

Fig. 4.4 Schematic diagram of the advancing and receding contact angles at the onset of droplet motion. Due to contact angle hysteresis, the contact angle above the actuated electrode is $\theta_{EW} + \alpha$ whilst the contact angle above the non-actuated electrode is $\theta_{eq} - \alpha$. For the droplet to move, $\theta_{EW} + \alpha < \theta_{eq} - \alpha$

Assuming V_{min} and α are small, then $\theta_{EW}(V_{min}) \rightarrow \theta_{eq}$ and (4.20) can be simplified to

$$V_{min} \approx 2\sqrt{\frac{\sigma_{lv}\alpha \sin\theta_{eq}}{C}} \tag{4.21}$$

where α is expressed in radians. It can be seen that a large dielectric capacitance, C, a large equilibrium contact angle, θ_{eq}, (i.e. a very hydrophobic surface), a small hysteresis angle, α, and a low surface tension, σ_{lv}, are desirable in order to minimise the actuation potential of the droplets.

4.2.3 AC Actuation

The theoretical descriptions of electrowetting discussed so far are applicable to the *static* conditions that occur in DC actuation. In the case of a very slowly varying AC voltage, the contact angle will follow the instantaneous value predicted by the Lippmann-Young equation. However, if the frequency of the applied AC voltage exceeds the hydrodynamic response frequency of the droplet, then the liquid will have insufficient time to adjust to the voltage variations, and the response then depends on the *time-averaged* voltage on the control electrode. (In EWOD applications involving millimetre-sized droplets, this will typically occur when the AC frequency exceeds approximately 100–200 Hz). Thus, in the case of AC droplet actuation, the voltage in the Lippmann-Young equation has to be replaced by the RMS (root-mean-square) value. As discussed by Mugele and Baret [31], the use of the Lippmann-Young equation for AC conditions is appropriate as long as the basic assumptions used to derive the equation are still valid. One of the most important assumptions is that the liquid can be treated as a perfect conductor. This is valid at low and moderate frequencies but above a critical frequency, ω_c, the liquid will start to behave as a dielectric, and the Lippmann-Young equation will begin to break down. The value of ω_c for a 10^{-4} M aqueous solution of NaCl is

of order 10^8 s^{-1} but demineralised water, for example, has a much lower value of $\omega_c \approx 4 \times 10^3$ s^{-1} [31].

AC actuation is often preferred for transporting solvents such as acetone, chloroform, dimethylformamide, ethanol, etc. since it has been found difficult or impossible to transport these liquids with DC voltages [64]. In addition, AC actuation has a number of other advantages including reduced dielectric hysteresis of the capacitance-voltage characteristics, and increased reliability by avoiding the build up of charges on the insulators. As a consequence, AC actuation has become the favoured method in most EWOD applications [14]. Actuation using a square wave is also considered a useful transport option in EWOD systems [92].

Section 4.2 has presented a brief overview of the theoretical considerations behind electro-wetting-on-dielectric actuation. In the interests of brevity, the descriptions of the underlying theory and the mathematical derivations have been kept as concise as possible. However, it is hoped that the reader will have obtained an increased awareness of the many subtleties that underpin electrowetting theory. For a more detailed description of the fundamentals of electrowetting, the reader is referred to the comprehensive review article by Mugele and Baret [31], and the appropriate chapters in Berthier [62] and Berthier and Silberzan [63]. In addition, there is now a growing volume of literature on the modelling and simulation of droplet-based electrowetting, with important work reported by Shapiro et al. [93], Zeng and Korsmeyer [94], Zeng [95], Lienemann et al. [96], Walker and Shapiro [97], Berthier et al. [69, 90], Lu et al. [98], Song et al. [99] and Clime et al. [100]. The main goal of the present chapter is to focus on the progress that has been made in the development of droplet-based electrowetting technologies for chemical and biological applications. The next section therefore discusses the various types of EWOD systems that are currently used in digital lab-on-a-chip applications.

4.3 Implementation of EWOD-Based Digital Microfluidics

EWOD-based microfluidic systems can be divided into two distinct categories depending on whether the system is open to the atmosphere or is covered. In open EWOD systems, the droplets are manipulated on a horizontal solid substrate which is exposed to the atmosphere, whereas in covered EWOD systems, the droplets are confined between two horizontal parallel plates, typically separated by a distance of between 50 and 200 μm. Each of these approaches has advantages and disadvantages. For example, it has been found that dispensing, transporting and splitting of droplets are best performed in covered EWOD systems, whereas droplet mixing and evaporation (so as to increase the concentration of the sample) are best performed in open EWOD systems [62].

Figure 4.5 illustrates a typical cross-section through a covered EWOD microfluidic chip. The lower plate of the chip contains the individual addressable electrodes and is usually fabricated from silicon or glass. The electrodes are then

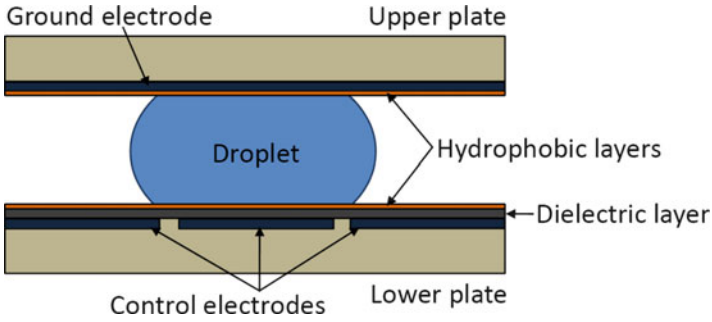

Fig. 4.5 A typical cross-section through a covered EWOD microfluidic chip

covered with a thin dielectric layer (Parylene, SiO_2 or Si_3N_4), typically about 1 μm in thickness, and finally the surface is coated with a highly hydrophobic layer (spin-coated Teflon or plasma deposited SiOC) to achieve an equilibrium contact angle larger than 90°. In closed EWOD systems, the upper confining plate usually contains a continuous electrode. Alternatively, the upper plate can be fabricated from conductive ITO (indium tin oxide) glass to provide the necessary electrical contact to the droplets. The upper plate is usually treated with the same hydrophobic coating as the lower plate, and the gap between the plates is generally filled with a silicone oil to prevent droplet evaporation and reduce surface contamination. In the case of open EWOD systems, the electrical contact to the droplets is achieved either through the use of a network of conducting wire electrodes (*catenae*) located a suitable distance above the surface of the chip [62, 69] or via the use of a *co-planar* design in which the lower plate contains both the buried activation electrodes and the contact electrodes [14, 101]. Co-planar designs have also been used successfully with closed EWOD systems; in this case, the upper conducting plate is simply replaced by a passive confining plate.

The basic concept of EWOD microfluidics is illustrated conceptually in Fig. 4.6. The chip is arranged with an array of equispaced control electrodes so that the droplets can be directed to various locations on the chip. In most applications, the electrodes are typically between 500 μm and 1 mm square, although considerable effort is currently being directed towards further miniaturisation of the technology. Sequential activation of the control electrodes creates zones of increased wettability which can be used to dispense, transport, split and merge the droplets in order to perform chemical and biological assays.

Many research groups have developed practical systems to implement EWOD-based droplet actuation. Some of the earliest demonstrations of EWOD microfluidic systems were presented by Pollack et al. [27, 29], Lee et al. [61], Moon et al. [102], Cho et al. [74], Paik et al. [103, 104] and Srinivasan et al. [105, 106]. Within a very short period of time, electrowetting technologies have developed to the point where it is now possible to conduct on-chip multiplexed assays to determine the concentration of target analytes. An example of a fully automated and integrated EWOD-based multiplexed lab-on-a-chip assay is shown in Fig. 4.7 which shows a pipelined glucose

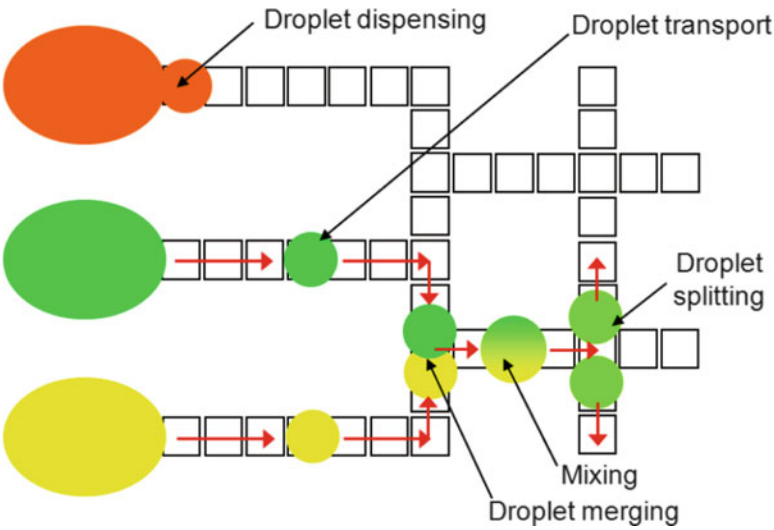

Fig. 4.6 Schematic representation of EWOD-based digital microfluidics showing each of the four main droplet handling operations: droplet dispensing, droplet transport, droplet merging and droplet splitting

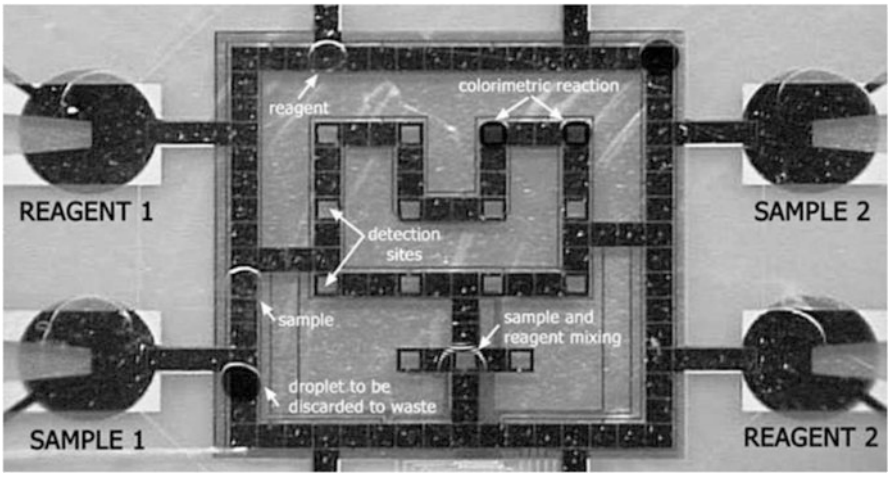

Fig. 4.7 Example of a fully automated and integrated EWOD-based system for conducting multiplexed lab-on-a-chip glucose assays. Reproduced from Srinivasan et al. [105] by permission of the Royal Society of Chemistry

assay developed by Srinivasan et al. [105]. In addition, Srinivasan et al. [107], Wheeler et al. [108] and Moon et al. [109] have demonstrated the use of EWOD-based systems for multiplexed proteomic sample preparation for high-throughput MALDI-MS (matrix assisted laser desorption/ionisation mass spectrometry).

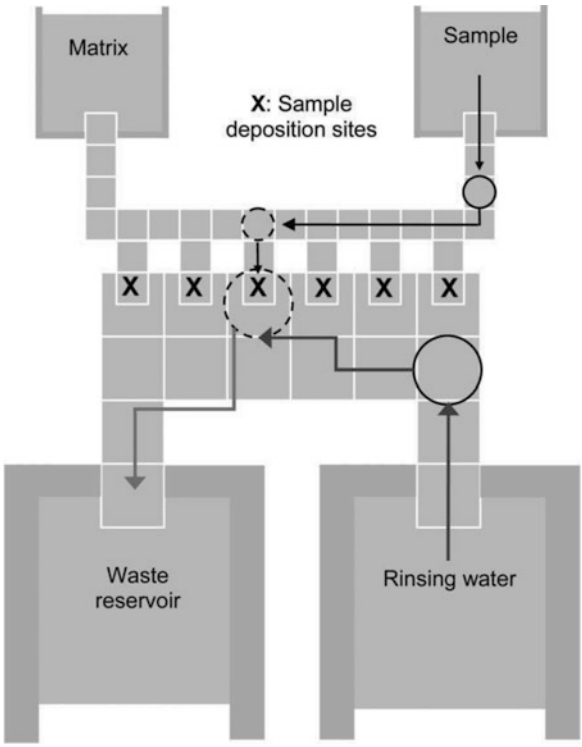

Fig. 4.8 Schematic view of an EWOD-based system for multiplexed sample preparation for MALDI-MS. Reproduced from Moon et al. [109] by permission of the Royal Society of Chemistry

Figure 4.8 shows a conceptual representation of the sample pre-treatment developed by Moon et al. [109] which consists of seven individual stages. Initially, droplets of the sample are dispensed from the sample reservoir and transported to the deposition sites where they are dried under vacuum for between 1 and 2 min. A series of water droplets are then dispensed from the rinsing water reservoir and moved over the protein deposition sites in order to remove any impurities from the samples; the rinsing droplets being discarded in the waste reservoir. Finally, droplets of 2,5-dihydroxybenzoic acid (DHB) are dispensed from the matrix reservoir and transported to the deposition sites where they are again dried under vacuum for between 1 and 2 min. After the drying stage is complete, the MALDI mass spectra can then be collected. The complex droplet handing protocols in this example serve to illustrate the huge potential of EWOD-based digital microfluidic systems for many laboratory procedures. However, one of the issues in developing fully-integrated digital microfluidic devices that can be used for chemical and biological assays is related to devising suitable protocols for the activation of the control electrodes. Some of the challenges of automating the droplet control operations in highly parallelised digital microfluidic chips have been addressed by Böhringer [110] and Griffith et al. [111].

One of the practical limitations of EWOD-based actuation is the requirement to fabricate a paved track of control electrodes beneath the surface of the microfluidic chip. In EWOD applications which require a large number of electrodes, it is

sometimes difficult to address each of the electrodes individually; this is especially the case if the electrical control circuitry is arranged on a single plane within the substrate of the chip. An elegant solution to the problem is the use of *multiplexing*, where groups of electrodes are attached to the same electrical control line. Multiplexing is particularly efficient for high-throughput parallel applications where the same droplet manipulation sequence is simultaneously performed on a large number of droplets. However, in some EWOD applications, there may be specific requirements to address all the electrodes separately. In this case, the control circuits need to use multiple conducting layers as found in IC (integrated-circuit) technologies. Gascoyne et al. [112] demonstrated the feasibility of individually addressing a large number of electrodes with a 32×32 programmable element dielectrophoresis chip based on CMOS (complementary metal-oxide-semiconductor) technology. More recently, Li et al. [113] have reported the integration of EWOD actuation on a standard CMOS chip. In addition, Gong and Kim [114] have investigated the use of EWOD-based systems fabricated from low-cost multilayer PCB (printed circuit board) substrates. Four different PCB post-processing methods were investigated, resulting in PCB-EWOD devices with varying degrees of performance and fabrication cost. The droplet handling operations on the best performing PCB substrate were found to be comparable to those on polished glass or silicon, making the PCB-EWOD approach valid for low-cost/disposable applications. A number of highly innovative, low-cost microfabrication approaches have also been developed by Abdelgawad and Wheeler [115, 116]. These enable EWOD systems to be manufactured without the use of specialist photolithographic and vapour deposition equipment, thus increasing the accessibility of EWOD technologies.

One of the most important parameters in EWOD devices is the voltage required to manipulate the droplets. Early EWOD applications typically required control voltages in the region of 80–100 V. However, by carefully selecting a dielectric material with a high relative permittivity, ε_d (both barium strontium titanate or bismuth zinc niobate appear to be very promising materials in this respect), and by carefully controlling the thickness of the dielectric layer, control voltages can be substantially reduced. This is enormously beneficial in EWOD applications due to the difficulties of implementing high-voltage CMOS technologies. The use of better dielectric materials has enabled EWOD-based droplet actuation to be reduced below 15 V in some applications [113].

Considerable effort is currently being directed towards improving the properties of the hydrophobic layer in order to create as large an equilibrium contact angle as possible. One of the most promising techniques for creating superhydrophobic surfaces is to pattern the substrate with nanostructured pillars [117]. Verplanck et al. [118] have studied a variety of wettability switching technologies for superhydrophobic surfaces, and have concluded that electrowetting droplet actuation is still the most promising approach compared to other control techniques such as optical, mechanical or thermal switching. However, electrowetting on superhydrophobic surfaces is still in its infancy and there are a number of problems to be overcome associated with the non-reversibility of the EWOD effect [62]. Another promising area for EWOD-based digital microfluidics is the development

of *all-terrain droplet actuation* (ATDA) [119] which removes the requirement to perform the droplet manipulation on a single horizontal plane. ATDA has been demonstrated for a wide range of non-planar geometries including inclined, vertical, twisted and upside-down surfaces and is a powerful technique that will enable the development of three-dimensional EWOD microfluidic systems, by stacking multiple layers on top of each other. In addition, ATDA should allow EWOD-based devices to be readily integrated into other microfluidic technologies. For example, Abdelgawad et al. [120] have recently demonstrated a hybrid device that integrates digital microfluidics and microchannels on the same substrate. This is an important step towards fully-integrated lab-on-a-chip systems for automatic sample processing and separation. Furthermore, Fan et al. [121] have demonstrated that ATDA technologies can be used to manipulate droplets against gravity around a flexible 8-in. (203 mm) long curved pathway, opening up the possibility of EWOD-based 'droplet-on-a-wristband' technologies for point-of-care applications.

4.4 Droplet Manipulation Using EWOD

The success of any microfluidic assay employing EWOD actuation relies crucially on the accuracy of the on-chip droplet handling operations which need to be precise, in terms of the volumes of the droplets produced, and repeatable over many operating cycles. It is therefore informative to consider each of the fundamental unit droplet operations in detail. However, before discussing the underlying theory and practical issues related to droplet manipulation, it is useful to assess the relative importance of the various forces that affect the droplets in EWOD devices.

4.4.1 Dimensional Considerations

In Sect. 4.2, the relative importance of the gravitational force to the surface tension force was shown to be expressed by the Bond number, Bo. In most electrowetting applications, the Bond number is usually less than unity, implying that gravitational forces are small in comparison to the surface tension forces. However, when dealing with droplets in motion, it is necessary to consider additional forces acting on the droplet, including the electrowetting, viscous and inertial forces. As previously discussed in Sect. 4.2, the strength of the electrowetting effect can be expressed by the dimensionless electrowetting number, $\eta = CV^2/(2\sigma_{\mathrm{lv}})$. In addition, the ratio between the viscous force and the inertial and surface tension forces in a droplet can be expressed by the non-dimensional Ohnesorge number, Oh [69]:

$$Oh = \frac{\mu}{\sqrt{\rho l \sigma_{\mathrm{lv}}}} \tag{4.22}$$

where μ is the dynamic viscosity of the liquid and l is the characteristic dimension of the droplet. Above a critical Ohnesorge number, $Oh_{\text{crit}} \approx 0.03$ [62], viscosity is found to play an important role in droplet handling operations. Considering a typical EWOD application using millimetre-sized droplets of water gives $\mu = 10^{-3}$ Ns/m^2, $\rho = 1,000$ kg/m^3, $l = 0.001$ m and $\sigma_{\text{lv}} = 0.072$ N/m—yielding an Ohnesorge number, $Oh \approx 4 \times 10^{-3}$ which is an order of magnitude less than the critical value of 0.03. This indicates that the effects of the viscosity of the liquid are generally quite small in most EWOD applications. However, it should be noted that in certain applications, involving highly viscous ionic liquids, the Ohnesorge number may exceed the critical value and the resulting droplet motion will then be significantly damped by the viscous forces.

It is also necessary to consider the ratio between the inertial and surface tension forces which can be determined from the non-dimensional Weber number, We [69]:

$$We = \frac{\rho v^2 l}{\sigma_{\text{lv}}} \tag{4.23}$$

where v is the velocity of the droplet. Above a critical Weber number, $We_{\text{crit}} \approx 1.1$ [62] the droplet will start to become distorted by the inertial forces and droplet break-up is a strong possibility [122]. Again, it is useful to consider the Weber number for typical EWOD applications involving millimetre-sized droplets. Experimental evidence indicates that droplet transport is relatively fast with typical transit times of order 20 ms to move a droplet between two adjacent electrodes spaced 800 μm apart [69]. This gives a characteristic velocity of approximately 0.04 m/s and leads to a Weber number (for a 1 mm diameter droplet) of $We = 0.022$ which is well below the critical value. Inertial effects are therefore relatively unimportant in most EWOD systems. However, in certain applications, surfactants are added to the liquid in order to allow easier spreading and splitting of the droplets. The addition of a surfactant reduces the liquid-vapour interfacial surface tension [123] and therefore increases the Weber number, making droplet distortion more likely.

The analysis of droplet motion often makes use of two further dimensionless numbers; the capillary number, Ca and the Reynolds number, Re. The capillary number expresses the ratio between the viscous and surface tension forces and is defined as

$$Ca = \frac{\mu v}{\sigma_{\text{lv}}} \tag{4.24}$$

However, the capillary number can be written in terms of the Ohnesorge and Weber numbers: $Ca = Oh\sqrt{We}$ and therefore the capillary number is not strictly an independent dimensionless parameter. Similarly, the Reynolds number expresses the ratio between the inertial and viscous forces and is defined as

$$Re = \frac{\rho v l}{\mu} \tag{4.25}$$

The Reynolds number can be also written in terms of the Ohnesorge and Weber numbers using the relationship: $Re = \sqrt{We}/Oh$. Consequently, EWOD-induced droplet handling is usually classified in terms of the Ohnesorge and Weber numbers.

4.4.2 Droplet Transport

Droplet motion in EWOD systems is carried out by sequentially activating the buried control electrodes one-at-a-time in order to set up suitable surface tension gradients on the surface of the microfluidic chip. This causes the droplets to move incrementally between neighbouring electrodes in accordance to changes in the electrowetting force. Since the Weber number in most EWOD applications is relatively low, the inertial forces acting on the droplets are generally small. Thus, the droplets will respond quickly to any changes in the electrowetting force and will rapidly accelerate up to a steady velocity before finally decelerating again once the droplets reach the target electrode. However, as discussed in Sect. 4.2.2.1, droplet motion can only be induced once the applied voltage exceeds a certain threshold voltage, $V_{\min}$, due to contact angle hysteresis. In practice, the threshold voltage can be reduced by immersing the droplets in silicone oil although the magnitude of the reduction in the threshold voltage has been found to depend on both the viscosity of the silicone oil as well as the viscosity of the liquid in the droplets [64]. Alternatively, simply exposing the surface of the chip to silicone oil and then drying has also been found to be effective at reducing the threshold voltage [64].

The droplet transport velocity is found to depend on the magnitude of the applied electrowetting force, as well as many other factors including the viscosity of the liquid, the electrowetting hysteresis angle and, in the case of covered EWOD systems, the separation distance between the upper and lower plates of the chip. An estimate of the maximum (steady-state) velocity of the droplet can be obtained by considering a simple force balance between the electrowetting force causing the motion and the viscous damping force due to the shear stress along the surface of the chip. In the case of covered EWOD systems, Berthier [62] has shown that the droplet velocity can be approximated by

$$v \approx \frac{h\sigma_{\mathrm{lv}}}{6\pi\mu r}\left(\cos\theta_{\mathrm{a}} - \cos\theta_{\mathrm{r}}\right) \tag{4.26}$$

where h is the separation between the upper and lower plates, r is the radius of the droplet in the horizontal plane, and θ_{a} and θ_{r} are the contact angles at the advancing and receding contact lines, given by $\theta_{\mathrm{a}} = \theta_{\mathrm{EW}} + \alpha$ and $\theta_{\mathrm{r}} = \theta_{\mathrm{eq}} - \alpha$, respectively. If the actuation voltage is less than the saturation voltage, and assuming that contact

angle hysteresis is small, then the Lippmann-Young equation can be substituted into (4.26) to obtain

$$v \approx \frac{h}{12\pi\mu r} CV^2 \tag{4.27}$$

indicating that the droplet velocity varies with the square of the applied voltage. Repeating the analysis using the modified Lippmann-Young equation (4.15) which accounts for contact angle saturation, leads to

$$v \approx \frac{h\sigma_{\mathrm{lv}}}{6\pi\mu r}(\cos\theta_{\mathrm{s}} - \cos\theta_{\mathrm{eq}})L\left(\frac{CV^2}{2\sigma_{\mathrm{lv}}(\cos\theta_{\mathrm{s}} - \cos\theta_{\mathrm{eq}})}\right) \tag{4.28}$$

where L is the Langevin function. Similar expressions to (4.26) and (4.27) can be derived for open EWOD systems, giving [62]:

$$v \approx \frac{4H\sigma_{\mathrm{lv}}}{5\pi\mu r}(\cos\theta_{\mathrm{a}} - \cos\theta_{\mathrm{r}}) = \frac{2H}{5\pi\mu r} CV^2 \tag{4.29}$$

where H is the maximum height of the droplet above the surface of the chip. The dynamics of EWOD-based droplet transport have been considered by a number of investigators including Ren et al. [124], Bahadur and Garimella [125], Chakraborty and Mittal [126], Baird et al. [127], Bavière et al. [128], Ahmadi et al. [129], Chatterjee et al. [130] and Song et al. [99].

4.4.2.1 Geometry of the Electrodes

Section 4.4.2 has shown how droplets can be transported across the substrate of a microfluidic chip using an incremental displacement from one electrode to the next. Ideally, the control electrodes should be placed as close as possible to each other in order to minimise the gap between the electrodes. Unfortunately, the method of fabrication often places a restriction on the proximity of the electrodes which usually have to be separated by a gap of between 10 and 30 μm, depending on the precision of the manufacturing process. The separation gap effectively creates a permanent hydrophobic halo around each electrode which can cause difficulties when trying to move a droplet to an adjacent electrode. This is especially the case in covered EWOD systems where the droplets are usually similar in size to the control electrodes. If a droplet comes to rest entirely within the perimeter of a single electrode, it becomes impossible to transport it any further, and the droplet is left permanently stranded or 'pinned' at the location.

An ingenious solution to the problem of droplet pinning is to incorporate jagged or crenellated edges around each of the electrodes, as shown in Fig. 4.9. The use of crenellated or inter-digitated electrodes ensures that at least part of the droplet

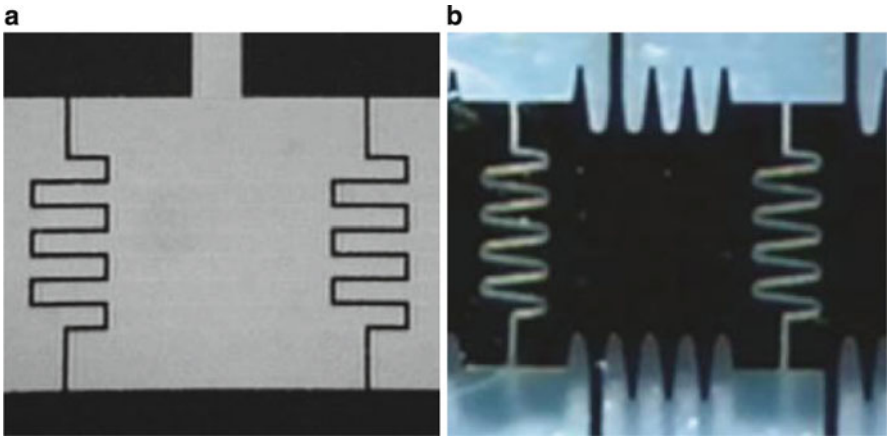

Fig. 4.9 Examples of crenellated and jagged electrode design. Reproduced from (**a**) Moon and Kim [132] with permission from Elsevier and (**b**) Pollack et al. [29] with permission from the Royal Society of Chemistry

extends onto the neighbouring electrode, thereby avoiding the problem of droplets becoming stranded. Clearly, the use of crenellations introduces additional complexity into the fabrication process but experimental evidence has shown that it is a very effective design strategy for aiding droplet motion. However, for the technique to be effective, the geometry and dimensions of the indentations have to be carefully selected. Berthier and Peponnet [131] have developed a detailed mathematical criterion that can be used to assess the effectiveness of the indentations, using the assumption that the crenellated edge can be approximated by a sinusoidal boundary. The effectiveness of the indentations can be found from the value of the function, G:

$$G(\lambda, e, \delta, n) = \frac{\lambda/e}{\delta/e + [\theta_1/\theta_2 - 1]/\pi n} \tag{4.30}$$

where λ is the size of the indentations, e is the width of the electrode, δ is the separation gap between the electrodes, n is the total number of indentations along one side of an electrode and θ_1 and θ_2 are the contact angles on the non-activated and activated electrodes, respectively. It should be noted, however, that not all EWOD applications make use of inter-digitated electrodes; a simple alternative is to ensure that the droplets are sufficiently large so that they always extend onto the adjacent electrodes.

4.4.3 Droplet Splitting and Merging

Splitting and merging are important droplet handling operations that are found in almost all EWOD applications. The basic principle of droplet splitting is illustrated

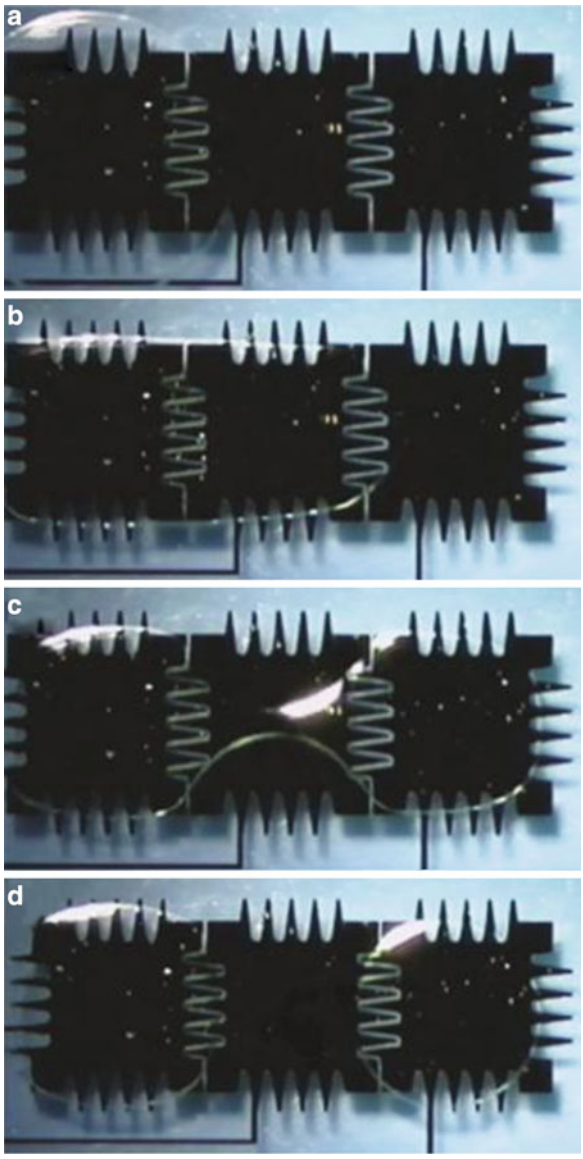

Fig. 4.10 Time-lapse sequence of images showing the successful splitting of a 900 nL droplet of 0.1 M KCl into two equal-sized daughter droplets in a covered EWOD system. Initially, only the left-hand electrode is energised (**a**). The middle electrode is then activated (**b**) and, after a short time delay, the voltage is switched from the middle to the right-hand electrode (**c**) resulting in division of the droplet (**d**). The electrodes are spaced at a pitch of 1.5 mm and the plate separation distance is 300 μm. The droplet is surrounded by 1 cSt silicone oil. Reproduced from Pollack et al. [29] by permission of the Royal Society of Chemistry

in Fig. 4.10 and involves three electrodes as described by Pollack et al. [29]. During the splitting process, the outermost electrodes are activated which reduces the contact angle. This creates two hydrophilic zones that stretch the droplet in the longitudinal direction. At the same time, the non-actuated central electrode is a hydrophobic region which tends to exert a 'pinching' force on the droplet which causes the neck of the droplet to split. In practice, splitting is very difficult to achieve in open EWOD systems since the droplet tends to 'escape' to one of the

hydrophilic electrodes. However, droplet splitting is feasible in covered EWOD systems, provided the plate separation distance is sufficiently small. By considering the pressure difference inside the droplet due to the different surface curvatures above the hydrophilic and hydrophobic electrodes, it is possible to show that for a square electrode of dimension, e, an approximate criterion for the maximum plate separation is given by [69]:

$$\frac{h_{\max}}{e} = -\cos\theta_{\text{eq}} \tag{4.31}$$

where it is assumed that the equilibrium contact angle, θ_{eq}, is larger than 90° so that $\cos\theta_{\text{eq}}$ is negative. Taking a typical EWOD system with a hydrophobic contact angle of $\theta_{\text{eq}} = 110°$ and 1 mm^2 electrodes, implies that the vertical separation of the plates should not exceed 340 μm. In practice, however, the plate separation is usually between 50 and 150 μm for 1 mm^2 electrodes.

A criterion for droplet splitting has been developed by Cho et al. [74] using Laplace's theorem [19, 31] to estimate the pressure within the droplet. Assuming that the principal radii of curvature of the droplet above the hydrophobic and hydrophilic electrodes are R_1 and R_2, respectively, then it can be shown that droplet splitting will occur when

$$\frac{R_2}{R_1} = 1 - \frac{R_2}{h}(\cos\theta_2 - \cos\theta_1) \tag{4.32}$$

where θ_1 and θ_2 are the contact angles on the non-activated (hydrophobic) and activated (hydrophilic) electrodes, respectively. The cutting operation is initiated by a pinching process in the middle of the droplet, yielding a concave contact line and a negative value of R_1. This condition can be achieved either by having a large value of $(\cos\theta_2 - \cos\theta_1)$ due to the electrowetting process, or by employing a small plate separation distance, h. It is interesting to note that the contact angle along the upper plate of the EWOD system does not affect the droplet splitting process. Neglecting contact angle hysteresis, then $\theta_1 = \theta_{\text{eq}}$ and $\theta_2 = \theta_{\text{EW}}$. The droplet splitting criterion can be then found by substituting the Lippmann-Young expression (4.11) into (4.32) to yield:

$$\frac{R_2}{R_1} = 1 - \frac{R_2}{h}\frac{\varepsilon_0\varepsilon_{\text{d}}V^2}{2d\sigma_{\text{lv}}} \tag{4.33}$$

The radius of curvature above the hydrophilic electrode, R_2, can be approximated from the size of the control electrode, e. At the point of droplet splitting $|R_1|$ is usually much larger than $|R_2|$ and hence the voltage required to split the droplet can be determined from (4.33). Recently, Song et al. [99] have presented a more detailed criterion for droplet splitting, based on the critical capillary number for droplet break-up, $Ca_{\text{crit}} \approx 10^{-3}$. In practice, the voltage required to split a droplet can also be determined by CFD (computational fluid dynamics) simulations.

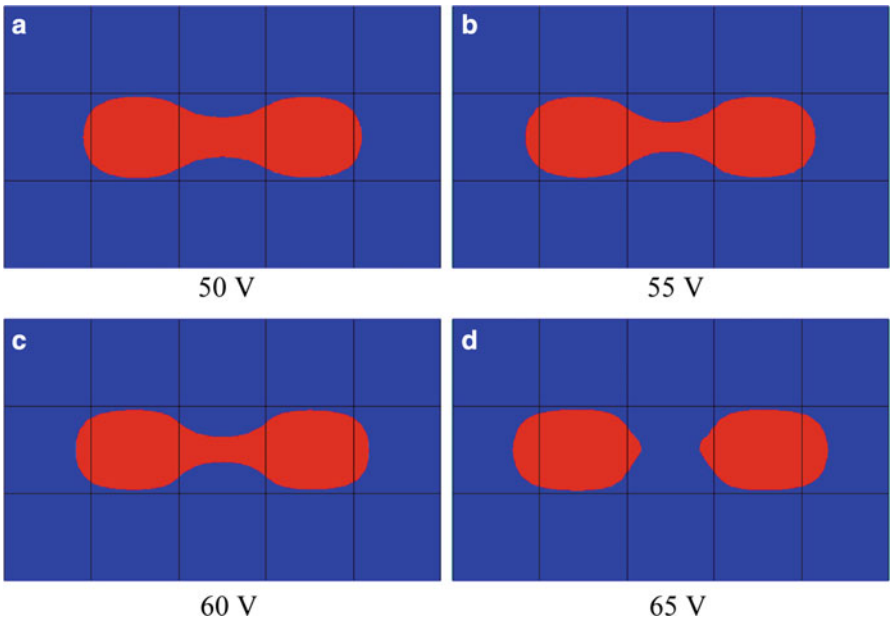

Fig. 4.11 Simulation of droplet splitting in a covered EWOD system using the commercial computational fluid dynamics (CFD) solver, CFD-ACE+ [133]. The images show the maximum elongation of the droplet as a function of applied voltage: (**a**) 50 V, (**b**) 55 V, (**c**) 60 V, (**d**) 65 V. Below a critical threshold voltage, the droplet fails to split

As an example, Fig. 4.11 shows the results of a simulation using the commercial CFD software tool, CFD-ACE+ [133]. The simulations allow the determination of the minimum actuation voltage for droplet splitting.

The merging of droplets in EWOD systems is an important handling operation since it enables the dilution of samples/reagents. For example, merging a sample droplet of concentration, C, with a buffer droplet of equal volume results in a droplet of twice the volume but with a concentration of $C/2$. Splitting this droplet then yields two droplets of concentration, $C/2$. By repeating this process of merging and then splitting the diluted droplets yields an exponential dilution of 2^N after N steps. Fortunately, the merging of droplets is relatively straightforward in EWOD systems and simply involves displacing the two droplets using electrowetting onto a common electrode. For applications involving aqueous liquids, the droplets generally coalesce very quickly due to the relatively high surface tension of water. However, the speed of coalescence is found to be reduced at higher Ohnesorge numbers.

One of the most challenging aspects when merging droplets is to ensure that the combined droplet is adequately mixed afterwards. This is especially important if the merging operation is part of a dilution assay. Droplet mixing is best performed in open EWOD systems since the presence of the confining plate in covered EWOD devices tends to suppress the natural droplet oscillations during the

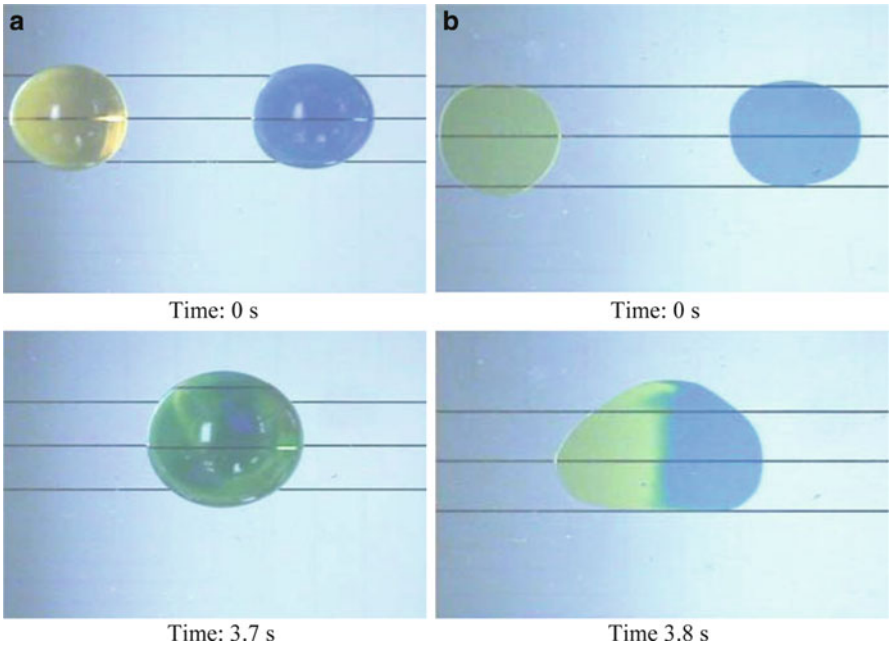

Fig. 4.12 Comparison of the mixing behaviour of two identically-sized droplets in an open EWOD system (**a**) and a covered EWOD system (**b**). Reproduced from Cooney et al. [134] with kind permission of Springer Science and Business Media

coalescence stage, thereby slowing the mixing processes [134]. The relatively poor mixing behaviour in covered EWOD systems is demonstrated in Fig. 4.12 which shows an experimental visualisation of the mixing following two identical droplet merging operations using an open and a covered EWOD system. Paik et al. [103, 104] have investigated a number of strategies to overcome the lack of mixing in covered EWOD systems. One possible remedy is to 'shuttle' the merged droplet backwards and forwards several times along a row of electrodes; the repeated changes in direction tend to increase the level of mixing inside the droplet. Alternatively, successive merging and splitting of the same droplet is also found to aid the mixing process. Another mixing strategy that is sometimes favoured is to transport the droplet in a looped motion, around a 2×2 or 2×4 array of electrodes, to promote a simultaneous stretching and folding motion in the liquid [104].

The success of any dilution study using repeated merging and splitting depends crucially on the reproducibility of the droplet volumes. The conventional 'three electrode splitting procedure', as described by Cho et al. [74], can lead to relatively large errors in the volumes of the individual droplets [14]. This in turn leads to significant errors in the accuracy of the dilution assay. To enhance the uniformity of the droplet splitting procedure, Ren [135] developed a novel electrode design which automatically aligns the droplet at the centre of the electrode. The design replaces

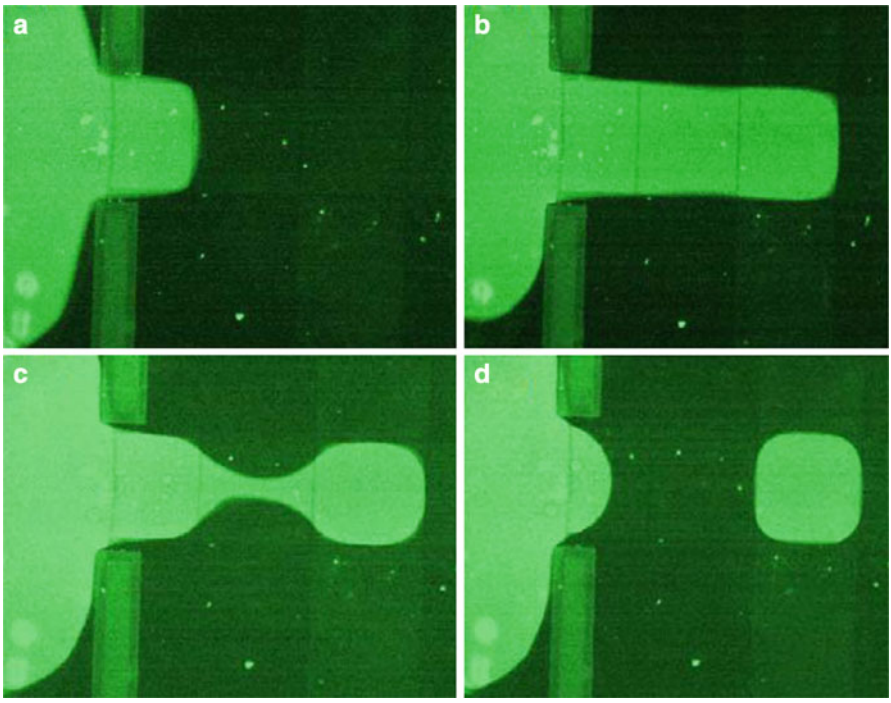

Fig. 4.13 Visualisation of droplet dispensing from a reservoir. The time-lapse sequence shows fluid being drawn out of the reservoir by activating the control electrodes immediately adjacent to the reservoir (**a, b**), the deactivation of the voltage on the 'cutting' electrode (**c**) and the 'back-pumping' stage (**d**). Reproduced from Berthier et al. [69] with kind permission from Elsevier

the single central electrode by three specially-shaped electrodes [14] that help guide the droplet into the correct symmetrical position. After droplet alignment, conventional side electrodes are then activated to complete the splitting process.

4.4.4 Droplet Dispensing

Droplet dispensing or droplet creation is the process of dividing a larger volume of liquid into smaller droplets that are suitable for manipulation within the EWOD system. As pointed out by Fair [14], droplet dispensing is one of the most crucial procedures in EWOD applications because it represents the interface from the macroscopic outside world to the microfluidic world within the chip. A typical droplet dispensing procedure is illustrated in Fig. 4.13 and is usually composed of three individual steps. Initially, the liquid is extruded from the reservoir by activating a number of electrodes to create a hydrophilic region that draws fluid out of the reservoir (see Fig. 4.13a, b). The extrusion of liquid is assisted by switching off the electrode(s) under the reservoir, creating a hydrophobic region

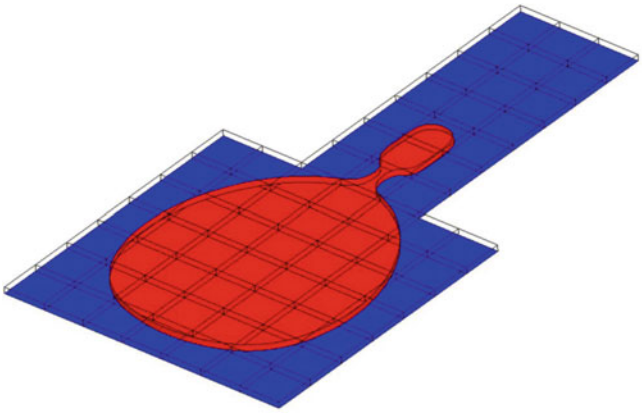

Fig. 4.14 Simulation of droplet dispensing from a reservoir using the commercial CFD solver, CFD-ACE+ [133]. The image shows the 'back-pumping' stage when the control electrode under the reservoir has been reactivated to reduce the pressure in the droplet in order to aid the cutting process

that tends to push fluid out of the reservoir. Once the extruded 'finger' of liquid has reached the electrode where the droplet is to be created, the voltage is deactivated on the 'cutting' electrode, causing a pinching effect as illustrated in Fig. 4.13c. In some applications, this pinching step is sufficient to create the droplet. However, a 'back-pumping' stage [62, 69] is sometimes used to assist the droplet formation process; this consists of reactivating the control electrode(s) under the reservoir to create either a hydrophilic ($\theta_{EW}<90°$) or a neutral ($90°<\theta_{EW}<95°$) contact angle. This reduces the pressure within the liquid which enhances the pinching effect, causing the droplet to detach from the main body of liquid. A detailed mathematical analysis of the criterion required for droplet detachment has been presented by Fair [14] and Song et al. [99]. Alternatively, the voltage required to draw liquid out of the reservoir and the voltage required for the back-pumping stage can be determined from CFD simulations. As an example, Fig. 4.14 shows the results of a numerical simulation using CFD-ACE+ [133] for determining the contact angle (and hence the required voltage) in the reservoir during the back-pumping stage. Experimental evidence and numerical simulations show that the magnitude of the surface tension, σ_{lv}, has very little effect on the droplet dispensing process [62, 69]. Instead, the main factor affecting the successful creation of droplets is the aspect ratio of the electrode size to plate separation distance, e/h. Droplet dispensing becomes easier as the value of e/h increases and it has been found that droplets can be created using a single cutting electrode when the ratio is larger than about six [14]. In some applications, the dispensing process can be assisted by incorporating a plastic wall to separate the reservoir from the main part of the fluidic chip [62, 69], as shown in Fig. 4.13.

EWOD microfluidic chips generally have a minimum of three reservoirs; one containing the sample, one for the reagent and the third for collecting the waste droplets once they have been analysed. In some applications, additional reservoirs

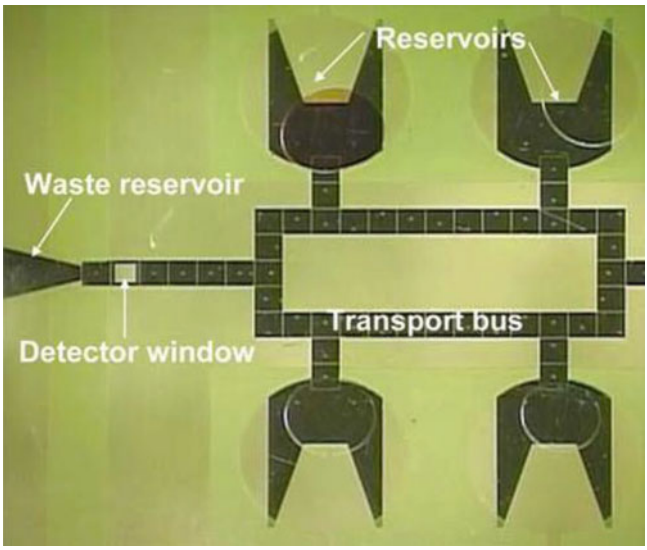

Fig. 4.15 An example of an EWOD multiplexed assay chip developed by Srinivasan [65] which contains one sample reservoir, one waste reservoir and three reagent reservoirs. Reproduced from Fair [14] with kind permission of Springer Science and Business Media

are needed to store a range of calibration solutions. An example of the layout of reservoirs on a typical EWOD system is shown in Fig. 4.15. One of the critical parameters affecting the overall reliability of EWOD systems is the shape of the electrode under the reservoir. This is important because the volume of liquid in the reservoir progressively decreases each time a droplet is dispensed. It is essential to ensure that the droplet in the reservoir is always in contact with the first working electrode along the dispensing track, otherwise the droplet creation mechanism will fail. One of the most popular designs for the reservoir electrode involves a tapered shape, as shown in Fig. 4.15. The tapered geometry is able to guide the droplet automatically into the correct position at the start of the dispensing track. In other applications, star-shaped electrodes have been found to be particularly effective at centralising the reservoir droplet at a predetermined location on the chip [69].

Section 4.4 has reviewed the fundamental EWOD droplet handling operations that are used in digital microfluidic systems. The final section of this chapter discusses how these individual operations can be integrated together to enable complex biological and chemical assays to be performed.

4.5 Chemical and Biological Applications of EWOD

One of the most common application areas for digital EWOD-based microfluidics is determining the concentration of target analytes in multiplexed assays, where multiple analytes are detected in a single sample. The fluidic steps usually involve

the following operations: (1) loading of the sample and reagents into the reservoirs, (2) dispensing droplets of the sample and reagent, (3) transport of the droplets to other parts of the chip, (4) mixing the sample and reagent droplets together, and (5) detection of the reaction products, either in-situ or remotely. In some applications, sample dilution, sample purification and particle separation may also be required. In most EWOD systems, the droplets containing the sample and the reagents, by necessity, have to be transported along the same fluidic tracks and consequently, there is potential for cross-contamination of the droplets. Experience has shown that non-biological electrolytes can be transported relatively easily, in both air and silicone oil, without cross-contamination being a major issue. However, the transport of droplets containing proteins, enzymes or human physiological fluids is more problematic due to the fact that biomolecules can sometimes bind nonspecifically to the hydrophobic layer, thus contaminating the surface of the chip. To avoid bio-fouling, silicone oil is normally used to isolate the droplet from the surface of the chip. In addition, proteins such as bovine serum albumin or casein are sometimes added to biological samples to reduce the level of nonspecific binding [62] while biocompatible surfactants such as Pluronic F127 can also be used to the limit the extent of protein adsorption [71]. Furthermore, experience suggests that the voltages required to perform the fundamental EWOD droplet handling operations are generally higher when the droplets contain biological macromolecules, proteins, cells or whole blood [62]. Despite these difficulties, a wide range of EWOD-based technologies have been developed. This section attempts to highlight some of the possible application areas in chemistry and biology.

4.5.1 EWOD-Based Glucose Assay

One of the first successful EWOD-based lab-on-a-chip devices for performing multiplexed assays was developed by Srinivasan et al. [105, 106] for determining the concentration of glucose in human physiological fluids. The device has already been illustrated in Fig. 4.7 of Sect. 4.3, and is based on a colorimetric enzyme-kinetic method based on Trinder's reaction [136]. The microfluidic device consists of fluid injection ports, reservoirs for the sample and reagents, fluidic tracks for droplet transport, an area for droplet mixing, and optical detection sites which use light-emitting-diodes (LEDs) and photodiodes to measure the absorbance of the sample. The glucose assay is performed as follows: droplets of the sample and reagent are dispensed from the appropriate reservoirs and then merged and mixed by shuttling the combined droplet across three electrodes for 15 s at a frequency of 8 Hz. After mixing, the droplet is then transported to the detection site where a photodiode measures the absorbance of the droplet at a wavelength of 545 nm for 30 s. The device is thus able to measure the concentration of glucose in less than 60 s and repeated measurements on the same sample concentration reveals changes in the measured concentration of less than 2%, indicating minimal variation in the

volumes of the droplets. Cross-contamination was avoided by filling the chip with silicone oil which effectively isolates the droplets from the Teflon AF hydrophobic layer.

4.5.2 EWOD-Based TNT Assay

Pamula et al. [137] have demonstrated the use of EWOD-based microfluidics for detecting nitroaromatic compounds such as commercial-grade 2,4,6-trinitrotoluene (TNT) or 2,4-dinitrotoluene (DNT). The most widely-accepted solvents for performing TNT analyses include acetone, acetonitrile or methanol. Unfortunately, none of these solvents are compatible with oil-based EWOD systems since they are miscible with silicone oil. To overcome this difficulty, Pamula et al. used dimethyl sulfoxide (DMSO) as the solvent since this dissolves nitroaromatic compounds whilst being immiscible with silicone oil. The basis of the assay involves reacting TNT or DNT with potassium hydroxide (KOH) to form coloured Jackson-Meisenheimer complexes [138] which can easily be detected on the chip using optical measurements in the UV and visible parts of the spectrum. Since the coloured complexes formed by reacting TNT and DNT with KOH are mutually independent, the assay is able to measure the concentration of TNT in the presence of DNT. The microfluidic chip developed by Pamula et al. was found to be capable of detecting TNT concentrations down to approximately 2.6 μg/mL.

4.5.3 EWOD-Based PCR Systems

The feasibility of EWOD-based polymerase chain reaction (PCR) devices was first demonstrated by Pollack et al. [139] for single-nucleotide polymorphisms (SNPs) and by Chang et al. [140] for a detection gene for the Dengue II virus. PCR involves the exponential amplification of fragments of DNA using a thermal cycling procedure which theoretically doubles the DNA concentration each cycle. At present, PCR is normally performed in large thermocycler systems that heat and cool 96-, 384- or 1536-well assay plates between three predetermined temperatures that are associated with the denaturation, annealing and extension phases of the DNA amplification process. One of the key advantages of being able to perform PCR in digital microfluidic systems is the ability to reduce the volume (and thereby cost) of the reagents and also to reduce the time taken to perform the thermal cycling due to the smaller thermal mass.

Pollack et al. [139] showed that the electrowetting actuation mechanism does not affect the PCR amplification process, thus demonstrating that EWOD can be used in PCR applications. In addition, they found that the higher ambient temperatures associated with PCR amplification tended to reduce the threshold voltage for droplet movement, enabling faster droplet transport. To date, most PCR-EWOD

systems apply the thermal cycling to the entire chip, allowing heating and cooling rates of between 1 and 2°C/s. However, alternative designs of EWOD chip are currently being investigated where the thermal regulation is performed on the chip itself to provide faster cycling times [62, 140]. One option is to use stationary droplets above a zone which is repeatedly heated and cooled while the other possibility is to transport the droplets between regions having different temperatures. A particularly promising technology for temperature regulation on EWOD chips is the use of mini-Peltier devices to cool (or heat) specific regions of the chip. However, there are a number of difficulties associated with PCR-EWOD systems. Firstly, the relatively high temperature of the denaturation stage (95°C) can lead to the formation of bubbles which disrupt the droplet transport mechanism and can also damage the dielectric layer. Rigorous de-gassing protocols are therefore essential in order to avoid problems with bubble formation. Evaporation is also a major issue at high temperatures and therefore it is essential that the droplets are surrounded by silicone oil. However, the main concern regarding EWOD-based PCR systems is the possibility of cross-contamination of DNA from one individual droplet to the next. Although cross-contamination can occur via the silicone oil, it is more likely to be caused by adsorption/desorption of the DNA on the hydrophobic layer of the chip. Pollack et al. [139] conducted experiments to ascertain the level of cross-contamination in a PCR-EWOD system, by repeatedly transporting DNA-containing and DNA-free droplets across a common electrode. After transporting the droplets for 45 min (and 75 thermal cycles), during which there were 15,000 separate opportunities for cross-contamination, little evidence was found for the transfer of DNA into the DNA-free droplets. Nevertheless, there are still some concerns regarding the problem of adsorption of DNA on to the surface of the chip, especially if the EWOD-chip is to be reused several times for different PCR assays.

4.5.4 EWOD-Based DNA Sequencing

Recent advances in digital microfluidics have opened up the possibility of performing DNA sequencing by synthesis. Figure 4.16 shows a prototype EWOD-based digital microfluidic device for DNA pyrosequencing that has been developed by *Advanced Liquid Logic* [14]. 'Sequencing-by-synthesis' involves taking the DNA strand of interest and synthesising its complementary strand enzymatically, one base pair at a time. The pyrosequencing method is based on detecting the activity of DNA polymerase (a DNA synthesising enzyme) using a chemiluminescent enzyme (luciferase). The assay is carried out by sequentially adding solutions of the four nucleotide bases—adenine (A), thymine (T), cytosine (C) and guanine (G) to the DNA sample of interest and detecting (by chemiluminescence) which of the nucleotides is added at each stage; this then allows the sequence of the unknown strand of DNA to be determined.

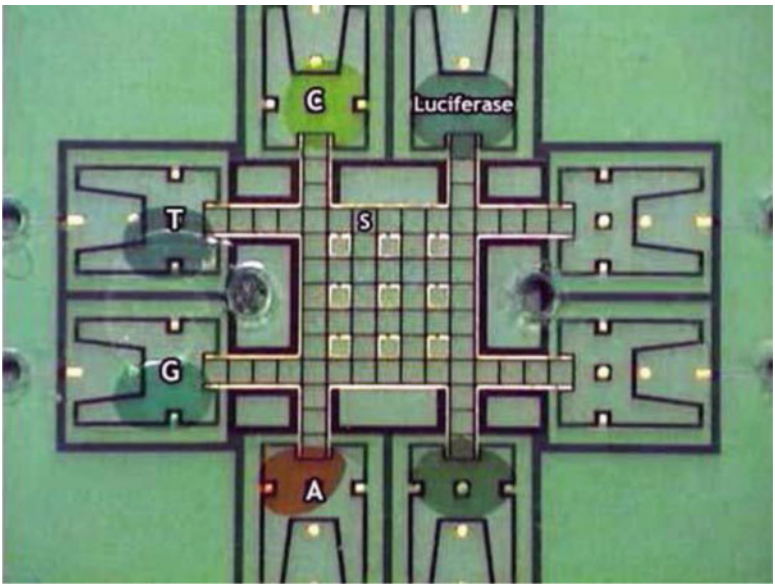

Fig. 4.16 Prototype DNA pyrosequencing chip developed by *Advanced Liquid Logic*. The chip contains reservoirs for dispensing solutions of A, T, C and G nucleotides and also a reservoir for the chemiluminescent enzyme (luciferase). The DNA is immobilised at location 'S'. Reproduced from Fair [14] with kind permission of Springer Science and Business Media

The operating sequence for the EWOD-based pyrosequencing chip involves dispensing a droplet containing one of the nucleotides (A, T, C or G) and transporting it to the site labelled 'S' containing the immobilised single-stranded DNA. The droplet is allowed to incubate at the site to allow time for polymerisation to take place, and is then transported away from the site and allowed to react with a droplet containing the chemiluminescent enzyme. After mixing, the combined droplet is transported to an optical sensor that detects chemiluminescent activity in the droplet. The system has no limitations on the number of bases than can be read since the synthesis and optical detection are physically separated on different parts of the chip. However, one of the practical difficulties appears to be the on-chip immobilisation of the DNA strand since the movement of the droplets over the site can cause the DNA molecules to be dislodged after many droplet operations. Nevertheless, the prototype EWOD-based pyrosequencing chip developed by *Advanced Liquid Logic* graphically demonstrates the power of digital microfluidic systems.

4.6 Future Trends and Concluding Remarks

Droplet handling technologies based on electrowetting have the potential to revolutionise many areas of analytical science by providing new functionalities and paradigms that are not possible in conventional laboratory procedures.

The recent developments in EWOD-based microfluidics have demonstrated that complex biological and chemical assays, including DNA and protein analyses, can be performed in digital microfluidic systems. EWOD-based microfluidic technologies are still very much in their infancy. However, the growing literature on EWOD droplet manipulation suggests that the technique will become an important technology in the development of the next generation of microfluidic devices.

Initial results have demonstrated that the use of digital microfluidics provides all the usual benefits associated with miniaturisation including smaller sample requirements, reduced reagent consumption, decreased analysis time, lower power consumption, lower costs per assay and higher levels of throughput and automation. However, the introduction of fully-controllable 'digital' microfluidic systems where the samples and reagents are manipulated using a standard set of droplet handling operations takes the technology beyond that which can be achieved using continuous flow microfluidics. The elegance of digital (droplet-based) microfluidics originates in the fact that the reactions or assays can be performed sequentially rather than as a continuous reaction, enabling complex chemical and biological protocols to be performed on a relatively simple microfluidic chip.

Undoubtedly, one of the factors that would make the use of electrowetting more attractive is further miniaturisation of the technology. The reduction in the volume of the droplets by scaling the control electrodes from the current dimensions (typically hundreds of microns) down to tens of microns, and the associated increase in the electrowetting switching speed will bring enormous benefits to EWOD-based applications. For example, miniaturisation of the technology would enable massively parallel DNA sequencing to be to be carried out, which would make sequencing a one million base-pair long genome feasible on a single microfluidic chip. Without doubt, further miniaturisation will be enormously challenging, not only due to the limitations and difficulties in device fabrication, but also due to fundamental issues associated with the fluid mechanics of micron-sized droplets. However, overcoming these challenges will enable EWOD-based digital microfluidic systems to play a major role in the next generation of microdroplet technologies.

References

1. Manz A, Becker H (1998) Microsystem technology in chemistry and life sciences: topics in current chemistry, vol 194. Springer, Berlin
2. Jakeway SC, de Mello AJ, Russell EL (2000) Miniaturized total analysis systems for biological analysis. Fresenius J Anal Chem 366:525–539
3. Squires TM, Quake SR (2005) Microfluidics: fluid physics at the nanoliter scale. Rev Mod Phys 77:977–1026
4. Whitesides GM (2006) The origins and the future of microfluidics. Nature 442:368–373
5. Tian W-C, Finehout E (2008) Microfluidics for biological applications. Springer, New York
6. Arora A, Simone G, Salieb-Beugelaar GB, Kim JT, Manz A (2010) Latest developments in micro total analysis systems. Anal Chem 82:4830–4847

7. Janasek D, Franzke J, Manz A (2006) Scaling and the design of miniaturized chemical-analysis systems. Nature 442:374–380
8. Karniadakis G, Beskok A, Aluru N (2005) Microflows and nanoflows: fundamentals and simulation. Springer, New York
9. Kockmann N (2008) Transport phenomena in micro process engineering. Springer, Berlin
10. de Mello AJ, Beard N (2003) Dealing with 'real' samples: sample pre-treatment in microfluidic systems. Lab Chip 3:11N–19N
11. Craighead H (2006) Future lab-on-a-chip technologies for interrogating individual molecules. Nature 442:387–393
12. Song H, Chen DL, Ismagilov RF (2006) Reactions in droplets in microfluidic channels. Angew Chem Int Ed 45:7336–7356
13. Haeberle S, Zengerle R (2007) Microfluidic platforms for lab-on-a-chip applications. Lab Chip 7:1094–1110
14. Fair RB (2007) Digital microfluidics: is a true lab-on-a-chip possible? Microfluid Nanofluid 3:245–281
15. Fair RB, Khlystov A, Tailor TD, Ivanov V, Evans RD, Srinivasan V, Pamula VK, Pollack MG, Griffin PB, Zhou J (2007) Chemical and biological applications of digital-microfluidic devices. IEEE Design Test Comput 24:10–24
16. Teh S-Y, Lin R, Hung L-H, Lee AP (2008) Droplet microfluidics. Lab Chip 8:198–220
17. Fouillet Y, Jary D, Chabrol C, Claustre P, Peponnet C (2008) Digital microfluidic design and optimization of classic and new fluidic functions for lab on a chip systems. Microfluid Nanofluid 4:159–165
18. Abdelgawad M, Wheeler AR (2009) The digital revolution: a new paradigm for microfluidics. Adv Mater 21:920–925
19. de Gennes P-G, Brochard-Wyart F, Quéré D (2004) Capillarity and wetting phenomena: drops, bubbles, pearls, waves. Springer, New York
20. Rosslee C, Abbott NL (2000) Active control of interfacial properties. Curr Opin Colloid Interface Sci 5:81–87
21. Lee J, Kim C-J (2000) Surface-tension-driven microactuation based on continuous electrowetting. J Microelectromech Syst 9:171–180
22. Darhuber AA, Troian SM (2005) Principles of microfluidic actuation by modulation of surface stresses. Annu Rev Fluid Mech 37:425–455
23. Gras SL, Mahmud T, Rosengarten G, Mitchell A, Kalantar-zadeh K (2007) Intelligent control of surface hydrophobicity. Chem Phys Chem 8:2036–2050
24. Lipowsky R (2001) Morphological wetting transitions at chemically structured surfaces. Curr Opin Colloid Interface Sci 6:40–48
25. Pfohl T, Mugele F, Seemann R, Herminghaus S (2003) Trends in microfluidics with complex fluids. Chem Phys Chem 4:1291–1298
26. Seemann R, Brinkmann M, Kramer EJ, Lange FF, Lipowsky R (2005) Wetting morphologies at microstructured surfaces. Proc Natl Acad Sci USA 102:1848–1852
27. Pollack MG, Fair RB, Shenderov AD (2000) Electrowetting-based actuation of liquid droplets for microfluidic applications. Appl Phys Lett 77:1725–1726
28. Quilliet C, Berge B (2001) Electrowetting: a recent outbreak. Curr Opin Colloid Interface Sci 6:34–39
29. Pollack MG, Shenderov AD, Fair RB (2002) Elecrowetting-based actuation of droplets for integrated microfluidics. Lab Chip 2:96–101
30. Mugele F, Klingner A, Buehrle J, Steinhauser D, Herminghaus S (2005) Electrowetting: a convenient way to switchable wettability patterns. J Phys Condens Matter 17:S559–S576
31. Mugele F, Baret J-C (2005) Electrowetting: from basics to applications. J Phys Condens Matter 17:R705–R774
32. Shamai R, Andelman D, Berge B, Hayes R (2008) Water, electricity, and between... On electrowetting and its applications. Soft Matter 4:38–45

33. Schwartz JA, Vykoukal JV, Gascoyne PRC (2004) Droplet-based chemistry on a programmable micro-chip. Lab Chip 4:11–17
34. Fan S-K, Hsieh T-H, Lin D-Y (2009) General digital microfluidic platform manipulating dielectric and conductive droplets by dielectrophoresis and electrowetting. Lab Chip 9:1236–1242
35. Wang K-L, Jones TB, Raisanen A (2009) DEP actuated nanoliter droplet dispensing using feedback control. Lab Chip 9:901–909
36. Darhuber AA, Valentino JP, Troian SM, Wagner S (2003) Thermocapillary actuation of droplets on chemically patterned surfaces by programmable microheater arrays. J Microelectromech Syst 12:873–879
37. Darhuber AA, Chen JZ, Davis JM, Troian SM (2004) A study of mixing in thermocapillary flows on micropatterned surfaces. Philos Trans R Soc Lond A 362:1037–1058
38. Darhuber AA, Valentino JP, Troian SM (2010) Planar digital nanoliter dispensing system based on thermocapillary actuation. Lab Chip 10:1061–1071
39. Chiou PY, Moon H, Toshiyoshi H, Kim C-J, Wu MC (2003) Light actuation of liquid by optoelectrowetting. Sens Actuators A 104:222–228
40. Chuang H-S, Kumar A, Wereley ST (2008) Open optoelectrowetting droplet actuation. Appl Phys Lett 93:064104
41. Chiou PY, Park S-Y, Wu MC (2008) Continuous optoelectrowetting for picoliter droplet manipulation. Appl Phys Lett 93:221110
42. Krogmann F, Qu H, Mönch W, Zappe H (2008) Push/pull actuation using optoelectrowetting. Sens Actuators A 141:499–505
43. Chiou PY, Chang Z, Wu MC (2008) Droplet manipulation with light on optoelectrowetting device. J Microelectromech Syst 17:133–138
44. Guttenberg Z, Müller H, Habermüller H, Geisbauer A, Pipper J, Felbel J, Kielpinski M, Scriba J, Wixforth A (2005) Planar chip device for PCR and hybridization with surface acoustic wave pump. Lab Chip 5:308–317
45. Beyssen D, Le Brizoual L, Elmazria O, Alnot P (2006) Microfluidic device based on surface acoustic wave. Sens Actuators B 118:380–385
46. Luo JK, Fu YQ, Li Y, Du XY, Flewitt AJ, Walton AJ, Milne WI (2009) Moving-part-free microfluidic systems for lab-on-a-chip. J Micromech Microeng 19:054001
47. Fu YQ, Luo JK, Du XY, Flewitt AJ, Li Y, Markx GH, Walton AJ, Milne WI (2010) Recent developments on ZnO films for acoustic wave based bio-sensing and microfluidic applications: a review. Sens Actuators B 143:606–619
48. Cho SK, Kim C-J (2003) Particle separation and concentration control for digital microfluidic systems. In: 16th IEEE annual international conference on MEMS, Kyoto, Japan, pp 686–689
49. Zhao Y, Yi U-C, Cho SK (2007) Microparticle concentration and separation by traveling-wave dielectrophoresis (twDEP) for digital microfluidics. J Microelectromech Syst 16:1472–1481
50. Cho SK, Zhao Y, Kim C-J (2007) Concentration and binary separation of microparticles for droplet-based digital microfluidics. Lab Chip 7:490–498
51. Fan S-K, Huang P-W, Wang T-T, Peng Y-H (2008) Cross-scale electric manipulations of cells and droplets by frequency-modulated dielectrophoresis and electrowetting. Lab Chip 8:1325–1331
52. Wang Y, Zhao Y, Cho SK (2007) Efficient in-droplet separation of magnetic particles for digital microfluidics. J Micromech Microeng 17:2148–2156
53. Sista RS, Eckhardt AE, Srinivasan V, Pollack MG, Palanki S, Pamula VK (2008) Heterogeneous immunoassays using magnetic beads on a digital microfluidic platform. Lab Chip 8:2188–2196
54. Shah GJ, Kim C-J (2009) Meniscus-assisted high-efficiency magnetic collection and separation for EWOD droplet microfluidics. J Microelectromech Syst 18:363–375

55. Nashida N, Satoh W, Fukuda J, Suzuki H (2007) Electrochemical immunoassay on a microfluidic device with sequential injection and flushing functions. Biosens Bioelectron 22:3167–3173
56. Sista R, Hua Z, Thwar P, Sudarsan A, Srinivasan V, Eckhardt A, Pollack M, Pamula V (2008) Development of a digital microfluidic platform for point of care testing. Lab Chip 8:2091–2104
57. Malic L, Brassard D, Veres T, Tabrizian M (2010) Integration and detection of biochemical assays in digital microfluidic LOC devices. Lab Chip 10:418–431
58. Lippmann G (1875) Relations entre les phénomènes électriques et capillaires. Ann Chim Phys 5:494–549
59. Berge B (1993) Electrocapillarity and wetting of insulator films by water. C R Acad Sci Paris, Série II 317:157–163
60. Vallet M, Berge B, Vovelle L (1996) Electrowetting of water and aqueous solutions on poly (ethylene terephthalate) insulating films. Polymer 37:2465–2470
61. Lee J, Moon H, Fowler J, Schoellhammer T, Kim C-J (2002) Electrowetting and electrowetting-on-dielectric for microscale liquid handling. Sens Actuators A 95:259–268
62. Berthier J (2008) Microdrops and digital microfluidics. William Andrew, Norwich, NY
63. Berthier J, Silberzan P (2010) Microfluidics for biotechnology, 2nd edn. Artech House, Boston
64. Pollack MG (2001) Electrowetting-based microactuation of droplets for digital microfluidics. PhD thesis, Duke University, USA
65. Srinivasan V (2005) A digital microfluidic lab-on-a-chip for clinical applications. PhD thesis, Duke University, USA
66. Chatterjee D, Hetayothin B, Wheeler AR, King DJ, Garrell RL (2006) Droplet-based microfluidics with nonaqueous solvents and solutions. Lab Chip 6:199–206
67. Brassard D, Malic L, Normandin F, Tabrizian M, Veres T (2008) Water–oil core-shell droplets for electrowetting-based digital microfluidic devices. Lab Chip 8:1342–1349
68. Probstein RF (1994) Physicochemical hydrodynamics: an introduction, 2nd edn. Wiley, New York
69. Berthier J, Clementz P, Raccurt O, Jary D, Claustre P, Peponnet C, Fouillet Y (2006) Computer aided design of an EWOD microdevice. Sens Actuators A 127:283–294
70. Yoon J-Y, Garrell RL (2003) Preventing biomolecular adsorption in electrowetting-based biofluidic chips. Anal Chem 75:5097–5102
71. Luk VN, Mo GCH, Wheeler AR (2008) Pluronic additives: a solution to sticky problems in digital microfluidics. Langmuir 24:6382–6389
72. Hayes RA, Feenstra BJ (2003) Video-speed electronic paper based on electrowetting. Nature 425:383–385
73. Washizu M (1998) Electrostatic actuation of liquid droplets for microreactor applications. IEEE Trans Ind Appl 34:732–737
74. Cho SK, Moon H, Kim C-J (2003) Creating, transporting, cutting, and merging liquid droplets by electrowetting-based actuation for digital microfluidic circuits. J Microelectromech Syst 12:70–80
75. Berge B, Peseux J (2000) Variable focal lens controlled by an external voltage: an application of electrowetting. Eur Phys J E 3:159–163
76. Kuiper S, Hendriks BHW (2004) Variable-focus liquid lens for miniature cameras. Appl Phys Lett 85:1128–1130
77. Dong L, Agarwal AK, Beebe DJ, Jiang H (2006) Adaptive liquid microlenses activated by stimuli-responsive hydrogels. Nature 442:551–554
78. Cattaneo F, Baldwin K, Yang S, Krupenkine T, Ramachandran S, Rogers JA (2003) Digitally tunable microfluidic optical fiber devices. J Microelectromech Syst 12:907–912
79. Levy U, Shamai R (2008) Tunable optofluidic devices. Microfluid Nanofluid 4:97–105
80. Chakrabarty K, Paik PY, Pamula VK (2007) Adaptive cooling of integrated circuits using digital microfluidics. Artech House, Boston

81. Peykov V, Quinn A, Ralston J (2000) Electrowetting: a model for contact-angle saturation. Colloid Polym Sci 278:789–793
82. Quinn A, Sedev R, Ralston J (2005) Contact angle saturation in electrowetting. J Phys Chem B 109:6268–6275
83. Papathanasiou AG, Boudouvis AG (2005) Manifestation of the connection between dielectric breakdown strength and contact angle saturation in electrowetting. Appl Phys Lett 86:164102
84. Mugele F (2009) Fundamental challenges in electrowetting: from equilibrium shapes to contact angle saturation and drop dynamics. Soft Matter 5:3377–3384
85. Krupenkin TN, Taylor JA, Schneider TM, Yang S (2004) From rolling ball to complete wetting: the dynamic tuning of liquids on nanostructured surfaces. Langmuir 20:3824–3827
86. Vallet M, Vallade M, Berge B (1999) Limiting phenomena for the spreading of water on polymer films by electrowetting. Eur Phys J B 11:583–591
87. Wang K-L, Jones TB (2005) Saturation effects in dynamic electrowetting. Appl Phys Lett 86:054104
88. Verheijen HJJ, Prins MWJ (1999) Reversible electrowetting and trapping of charge: model and experiments. Langmuir 15:6616–6620
89. Chen JZ, Troian SM, Darhuber AA, Wagner S (2005) Effect of contact angle hysteresis on thermocapillary droplet actuation. J Appl Phys 97:014906
90. Berthier J, Dubois P, Clementz P, Claustre P, Peponnet C, Fouillet Y (2007) Actuation potentials and capillary forces in electrowetting based microsystems. Sens Actuators A 134:471–479
91. Keshavarz-Motamed Z, Kadem L, Dolatabadi A (2010) Effects of dynamic contact angle on numerical modeling of electrowetting in parallel plate microchannels. Microfluid Nanofluid 8:47–56
92. Fan S-K, Yang H, Wang T-T, Hsu W (2007) Asymmetric electrowetting—moving droplets by a square wave. Lab Chip 7:1330–1335
93. Shapiro B, Moon H, Garrell RL, Kim C-J (2003) Equilibrium behavior of sessile drops under surface tension, applied external fields, and material variations. J Appl Phys 93:5794–5811
94. Zeng J, Korsmeyer T (2004) Principles of droplet electrohydrodynamics for lab-on-a-chip. Lab Chip 4:265–277
95. Zeng J (2006) Modeling and simulation of electrified droplets and its application to computer-aided design of digital microfluidics. IEEE Trans Comput Aid Des Integr Circ Syst 25:224–233
96. Lienemann J, Greiner A, Korvink JG (2006) Modeling, simulation, and optimization of electrowetting. IEEE Trans Comput Aid Des Integr Circ Syst 25:234–247
97. Walker SW, Shapiro B (2006) Modeling the fluid dynamics of electrowetting on dielectric (EWOD). J Microelectromech Syst 15:986–1000
98. Lu H-W, Glasner K, Bertozzi AL, Kim C-J (2007) A diffuse-interface model for electrowetting drops in a Hele-Shaw cell. J Fluid Mech 590:411–435
99. Song JH, Evans R, Lin Y-Y, Hsu BN, Fair RB (2009) A scaling model for electrowetting-on-dielectric microfluidic actuators. Microfluid Nanofluid 7:75–89
100. Clime L, Brassard D, Veres T (2010) Numerical modeling of electrowetting transport processes for digital microfluidics. Microfluid Nanofluid 8:599–608
101. Yi U-C, Kim C-J (2006) Characterization of electrowetting actuation on addressable single-sided coplanar electrodes. J Micromech Microeng 16:2053–2059
102. Moon H, Cho SK, Garrell RL, Kim C-J (2002) Low voltage electrowetting-on-dielectric. J Appl Phys 92:4080–4087
103. Paik P, Pamula VK, Pollack MG, Fair RB (2003) Electrowetting-based droplet mixers for microfluidic systems. Lab Chip 3:28–33
104. Paik P, Pamula VK, Fair RB (2003) Rapid droplet mixers for digital microfluidic systems. Lab Chip 3:253–259
105. Srinivasan V, Pamula VK, Fair RB (2004) An integrated digital microfluidic lab-on-a-chip for clinical diagnostics on human physiological fluids. Lab Chip 4:310–315

106. Srinivasan V, Pamula VK, Fair RB (2004) Droplet-based microfluidic lab-on-a-chip for glucose detection. Anal Chim Acta 507:145–150
107. Srinivasan V, Pamula V, Paik P, Fair R (2004) Protein stamping for MALDI mass spectrometry using an electrowetting-based microfluidic platform. In: Lab-on-a-chip: platforms, devices, and applications. Proceedings of SPIE, vol 5591, Philadelphia, Pennsylvania (PA), USA, pp 26–32
108. Wheeler AR, Moon H, Bird CA, Loo RRO, Kim C-J, Loo JA, Garrell RL (2005) Digital microfluidics with in-line sample purification for proteomics analyses with MALDI-MS. Anal Chem 77:534–540
109. Moon H, Wheeler AR, Garrell RL, Loo JA, Kim C-J (2006) An integrated digital microfluidic chip for multiplexed proteomic sample preparation and analysis by MALDI-MS. Lab Chip 6:1213–1219
110. Böhringer KF (2006) Modeling and controlling parallel tasks in droplet-based microfluidic systems. IEEE Trans Comput Aid Des Integr Circ Syst 25:334–344
111. Griffith EJ, Akella S, Goldberg MK (2006) Performance characterization of a reconfigurable planar-array digital microfluidic system. IEEE Trans Comput Aid Des Integr Circ Syst 25:345–357
112. Gascoyne PRC, Vykoukal JV, Schwartz JA, Anderson TJ, Vykoukal DM, Current KW, McConaghy C, Becker FF, Andrews C (2004) Dielectrophoresis-based programmable fluidic processors. Lab Chip 4:299–309
113. Li Y, Parkes W, Haworth LI, Stokes AA, Muir KR, Li P, Collin AJ, Hutcheon NG, Henderson R, Rae B, Walton AJ (2008) Anodic Ta_2O_5 for CMOS compatible low voltage electrowetting-on-dielectric device fabrication. Solid State Electron 52:1382–1387
114. Gong J, Kim C-J (2008) Direct-referencing two-dimensional-array digital microfluidics using multilayer printed circuit board. J Microelectromech Syst 17:257–264
115. Abdelgawad M, Wheeler AR (2007) Rapid prototyping in copper substrates for digital microfluidics. Adv Mater 19:133–137
116. Abdelgawad M, Wheeler AR (2008) Low-cost, rapid-prototyping of digital microfluidics devices. Microfluid Nanofluid 4:349–355
117. Herbertson DL, Evans CR, Shirtcliffe NJ, McHale G, Newton MI (2006) Electrowetting on superhydrophobic SU-8 patterned surfaces. Sens Actuators A 130–131:189–193
118. Verplanck N, Coffinier Y, Thomy V, Boukherroub R (2007) Wettability switching techniques on superhydrophobic surfaces. Nanoscale Res Lett 2:577–596
119. Abdelgawad M, Freire SLS, Yang H, Wheeler AR (2008) All-terrain droplet actuation. Lab Chip 8:672–677
120. Abdelgawad M, Watson MWL, Wheeler AR (2009) Hybrid microfluidics: a digital-to-channel interface for in-line sample processing and chemical separations. Lab Chip 9:1046–1051
121. Fan S-K, Yang H, Hsu W (2011) Droplet-on-a-wristband: chip-to-chip digital microfluidic interfaces between replaceable and flexible electrowetting modules. Lab Chip 11:343–347
122. Duan R-Q, Koshizuka S, Oka Y (2003) Two-dimensional simulation of drop deformation and breakup at around the critical Weber number. Nucl Eng Des 225:37–48
123. Raccurt O, Berthier J, Clementz P, Borella M, Plissonnier M (2007) On the influence of surfactants in electrowetting systems. J Micromech Microeng 17:2217–2223
124. Ren H, Fair RB, Pollack MG, Shaughnessy EJ (2002) Dynamics of electro-wetting droplet transport. Sens Actuators B 87:201–206
125. Bahadur V, Garimella SV (2006) An energy-based model for electrowetting-induced droplet actuation. J Micromech Microeng 16:1494–1503
126. Chakraborty S, Mittal R (2007) Droplet dynamics in a microchannel subjected to electrocapillary actuation. J Appl Phys 101:104901
127. Baird E, Young P, Mohseni K (2007) Electrostatic force calculation for an EWOD-actuated droplet. Microfluid Nanofluid 3:635–644

128. Bavière R, Boutet J, Fouillet Y (2008) Dynamics of droplet transport induced by electrowetting actuation. Microfluid Nanofluid 4:287–294
129. Ahmadi A, Najjaran H, Holzman JF, Hoorfar M (2009) Two-dimensional flow dynamics in digital microfluidic systems. J Micromech Microeng 19:065003
130. Chatterjee D, Shepherd H, Garrell RL (2009) Electromechanical model for actuating liquids in a two-plate droplet microfluidic device. Lab Chip 9:1219–1229
131. Berthier J, Peponnet C (2007) A model for the determination of the dimensions of dents for jagged electrodes in electrowetting on dielectric microsystems. Biomicrofluidics 1:014104
132. Moon I, Kim J (2006) Using EWOD (electrowetting-on-dielectric) actuation in a micro conveyor system. Sens Actuators A 130–131:537–544
133. CFD-ACE+ (2008) User manual: version 2008.2. ESI CFD, Inc., Huntsville, AL
134. Cooney CG, Chen C-Y, Emerling MR, Nadim A, Sterling JD (2006) Electrowetting droplet microfluidics on a single planar surface. Microfluid Nanofluid 2:435–446
135. Ren H (2004) Electrowetting-based sample preparation: an initial study for droplet transportation, creation and on-chip digital dilution. PhD thesis, Duke University, USA
136. Trinder P (1969) Determination of blood glucose using 4-amino phenazone as oxygen acceptor. J Clin Pathol 22:246
137. Pamula VK, Srinivasan V, Chakrapani H, Fair RB, Toone EJ (2005) A droplet-based lab-on-a-chip for colorimetric detection of nitroaromatic explosives. In: 18th IEEE international conference on MEMS, Miami Beach, FL, USA, pp 722–725
138. Terrier F (1982) Rate and equilibrium studies in Jackson-Meisenheimer complexes. Chem Rev 82:78–152
139. Pollack MG, Paik PY, Shenderov AD, Pamula VK, Dietrich FS, Fair RB (2003) Investigation of electrowetting-based microfluidics for real-time PCR applications. In: Seventh international conference on miniaturized chemical and biochemical analysis systems—proceedings of the 2003 MicroTAS conference, Squaw Valley, CA, pp 619–622
140. Chang Y-H, Lee G-B, Huang F-C, Chen Y-Y, Lin J-L (2006) Integrated polymerase chain reaction chips utilizing digital microfluidics. Biomed Microdevices 8:215–225